



---

Msc Thesis

---

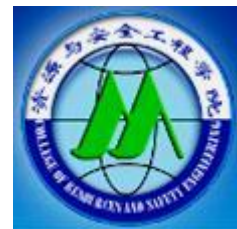
**The Development of Fractures in Overlying Strata and  
Design of Methane Drainage on 2874W working face  
Qianjiaying Coal Mine**

---

**Author: Gulzhan Yedigeyeva**

**Supervisor: Professor Hongqing Zhu**

(07/06/2018)



---

School of Resources and Safety Engineering  
China University of Mining and Technology (Beijing)

Xueyuan Rd, Ding 11, Haidian district, Beijing  
Zhonghe Building, 225

---

## **Declaration of Authorship**

---

„I declare in lieu of oath that this thesis is entirely my own work except where otherwise indicated. The presence of quoted or paraphrased material has been clearly signaled and all sources have been referred. The thesis has not been submitted for a degree at any other institution and has not been published yet.”

Gulzhan Yedigeyeva

---

## Abstract

---

One of the most fatal accidents taking place in Chinese coal mines are gas accidents. The measures of gas control and identification of high methane accumulation region are essential for underground coal mines. Moreover, bigger demands for coal resulted in mining at higher depths with low permeability. However, it was found out that longwall mining causes formation of de-stressed zone in the overlying strata, which increases the permeability. Fractures in the de-stressed zone act as pathways for liberated gas to flow to, thus, forming a zone of high methane accumulation in the overlying strata above longwall panel. The working face 2874W of Qianjiaying Coal Mine was chosen as case study of this research paper. To investigate the height of fractured zone in the overlying strata, three-dimensional numerical simulation model using finite element code FLAC3D software was carried out. The results of the simulation displayed the zone in the overlying strata where fractures are expected to occur along with approximate height of fractured zone. What is more, computational fluid dynamics CFD FLUENT was implemented to investigate the region of high methane concentration in goaf. The results of the simulation showcased the region in goaf (upper corner) with high methane concentration and regional low velocity of air in that zone. Moreover, based on the results of simulation results of FLAC3D and FLUENT, theoretical guidance on methane drainage using high-level and low-level borehole arrangements to drain gas in the overlying strata of goaf and installation of buried pipe in the upper corner of the goaf on 2874W working face was proposed in accordance with gas drainage experience in Chinese coal mines.

---

## Table of Contents

---

Declaration of Authorship .....	II
Abstract.....	III
Table of Contents .....	IV
1 Introduction.....	1
1.1 Research background .....	1
1.2 Research status .....	2
1.3 Main objective of the research .....	4
2 Location and general description .....	5
2.1 Location.....	5
2.2 Description of working face.....	5
2.3 Fault and folds.....	6
2.4 Mine gas sources .....	7
3 Simulation the response of overlying strata to longwall mining using FLAC3D.....	8
3.1 Formation of three zones.....	8
3.2 Stress zones division .....	10
3.3 The relationship between permeability and fracture.....	11
3.4 Simulation by FLAC3D .....	12
3.4.1 Geometry of the model.....	12
3.4.2 Description of the model.....	13
3.4.3 Boundary conditions and parameters .....	15
3.5 Results .....	16
3.5.1 Vertical stress distribution.....	16
3.5.2 Vertical displacement.....	21
3.5.3 Plastic damage state of the model .....	25
3.6 Summary .....	29
4 Simulation of gas migration in goaf by FLUENT .....	31
4.1 Geometry of the model.....	31
4.2 Boundary conditions .....	32
4.3 Gas seepage characteristics .....	33
4.4 Gas governing equations .....	34
4.5 Results of the simulation.....	35

4.5.1	Velocity distribution.....	35
4.5.2	The mass fraction of methane distribution.....	37
4.5.3	Pressure distribution.....	38
4.6	Summary .....	39
5	The design of the methane drainage .....	40
5.1	Formation of annular fissure circle .....	40
5.2	The principle of high level drill hole.....	41
5.3	Selection of drilling location.....	41
5.4	High level drill hole parameters design .....	42
5.5	The design of drill holes.....	43
5.5.1	Calculation of drilling parameters for high-level drill hole .....	45
5.6	Design of pipe in the upper corner .....	54
5.6.1	Calculation of design parameters .....	54
5.7	Summary .....	56
6	Summary and conclusions .....	57
7	Bibliography .....	59
8	List of Figures .....	63
9	List of Tables .....	65

---

# 1 Introduction

---

Gasification of coal takes place due to “parallel-consecutive” chemical reactions between gasifying agents and carbon-based part of the coal under circumstance of high temperature (Cempa-Balewicz et al., 2013).

Coal mine methane (CMM) is a term for all methane gas released in the course of or after mining activities either from the coal seam or from other gassy formations underground (Karacan, 2011).

---

## 1.1 Research background

---

The main reason of concern with methane in underground coal mines due to gas accidents is safety concern. Gas accidents are major fatalities taking place in Chinese coal mines (Guo and Yuan, 2015; Wang, Cheng and Liu, 2014; Zhang et al., 2018(a)). To ensure safety in underground coal mines gas drainage with determination of zone of high methane concentration in goaf is needed.

Not only is methane getting attention because of safety concerns, but also CMM contributes to fugitive greenhouse gas emissions and is an additional source of clean energy, which will be dissipated if not utilized (Guo and Yuan, 2015; Karacan, 2011).

Moreover, the trend for bigger demands for coal, higher production levels and therefore mining of coal seams that are more remote from the surface provoked increased attention to methane drainage (Moll, 1993).

The result of extraction of coal at higher depths leads to the phenomenon of low permeability of coal seams (Karacan et al., 2011; Chen et al., 2014) in (Zhang et al., 2018(b)).

Underground longwall extraction of coal instigates great extent of disturbance to the rock mass surrounding the excavated area. The changes in stress and fissuring caused by mining can increase permeability and also release methane from the strata in the vicinity of the excavation (Esterhuizen and Karacan, 2005).

The gas in the goaf area undergoes desorption from coal matrix, dissipation, followed by permeation and lastly accumulation. Eventually, a zone is brought into being where the concentration of methane is high and into which methane easily flows into (Zhang et al., 2012). This zone is named fractured zone.

Depending on borehole arrangement and other operation parameters, the gas pumped out from the fissures in the overlying strata above goaf may contain methane in the content of 30-95 % (Karacan, 2009) in (Karacan, 2011). Therefore, the research about fissures in the overlying strata of goaf is paramount for the guidelines of methane drainage.

This research will focus on draining the gas from region in goaf known for high methane concentration.

---

## **1.2 Research status**

---

Over the years, researchers used different methods to investigate the fractures of overlying strata of goaf. For instance, Xu, Zhang and Tian (2012) studied the development law of fissures in overlying strata through field measurement and performing physical simulation. While Researchers (Wang et al.,2017) accessed the height of fractured zone by quantitatively analyzing the correlation between porosity distribution and development of fissures in the overlying strata of goaf.

Many researchers have approached the extent of fractured zone through empirical and field observations (Palchik, 1989; Karmis et al., 1983; Palchik,2002) indicating that the extent of fractured zone is dependent on the thickness of coal seam. For instance, (Palchik, 2002) suggested that when the overlying rock strata is weak and porous, the height of the caved zone can reach 4 to 11 times the height of the coal seam.

To date, number of researchers investigated the de-stressed zone in overlying strata by numerical simulation (Xu et al., (2010); Duan and Xu (2012); Sui et al., (2014); Follington and Isaac, (1990); Shi and Liu, 2008). For instance, the research by Xu et al., (2010) provided information on the extent of fractured zone in overburden strata and rock failure through establishing numerical simulation model by means of FLAC3D. The ground response in the form of deformation was simulated through establishing numerical simulation using FLAC3D determining height of fractured zone by Duan and Xu (2012). Zhao et al. (2015) accessed the height of fractured zone induced by mining in the overlying strata by coupling results FLAC3D and GIS. The previous research provided paramount information about gas-enriched zone in the overlying the goaf strata.

The augmentation of permeability is connected to the stress change path and experienced damage (Fortin et al., 2005; Wang, Elsworth and Liu, (2013)). Extensive

research was placed to characterize the strata stress changes due to longwall mining and associated change in permeability. A comprehensive study executed by (Guo et al. 2012) investigated strata movement due to longwall mining, dynamic development of stress, the resultant changes in fractures establishing relationship between permeability and de-stressing and fracturing by three dimensional finite element code. Research by (Meng, Shi and Li, 2016) implemented FLAC3D for simulation of stress field and mining-induced rock failure around excavated area with the results acquiring permeability coefficient. (Karacan et al. 2007) established "dynamic" reservoir model to examine the goaf gas flow, using FLAC-2D as a software to observe the change in fractured rock permeability in overlying strata of the longwall panel.

In order to simulate the fluid dynamics, modelling using computational fluid dynamics code made possible to observe inaccessible the "unseen" happening inside goaf (Balusu et al., 2002; Karacan et al., 2007; Yuan et al., 2006) in (Qin et al., 2015). Interested in flow of methane in goaf number of researchers investigated the flow by means of CFD simulation (Guo et al., 2015; Zhang, 2012; Qin et al., 2015; Guo et al., 2012; Guo and Yuan, 2015). (Qin et al. 2015) in their study simulated the flow of gas by means of geomechanical model of mining-induced rock strata integrated into CFD model using FLUENT software. The work of previous researchers provided some understanding of goaf gas flow pattern as well as displayed various implementations of computational fluid dynamics used to study fluid dynamics through porous medium of goaf.

With the aim of optimizing gas drainage production (Ding, Jiang and Zhu, 2012; Whittles et al., 2006; Li, 2013; Nie, 2008; Li, 2018; Zhang et al., 2011; Tian-xuan, Zhi-chao and Feng, 2012) by various means proposed parameters needed for gas drainage. For instance, (Whittles et al. 2006) simulated gas flow and geomechanical changes underwent in active coal production panel using FLAC commercial software, presenting information on presence of fissures that can act as potential gas sources along with fissures flow paths of gas into longwall mine workings.

Even though the previous research provided paramount understanding of the movement and deformation of overlying strata as well as fluid dynamics and position of placement of boreholes, site-specific simulation is needed to accommodate the plan of design of methane drainage. So, based on the cite conditions in the Qianjiaying coal mine this research will attempt at providing information on gas drainage according to the



overburden strata change due to mining and identifying the high methane zone in goaf implementing the goaf gas drainage there.

---

### **1.3 Main objective of the research**

---

Working face number 2874 W of Qianjiaying coal mine is chosen as a case study for this research paper. This work puts its aim to investigate the extent of cracks the overlying strata formed as a response to the longwall mining as well as identifying possible accumulation region of high methane concentration in the goaf. Analyzing the results of fractured zone extent and zone of high gas concentration, the theoretical guidance on methane drainage design will be proposed.

The height of the fractured zone of overlying the goaf strata is acquired through simulation using FLAC3D software to do so. This is done by analyzing the evolution of vertical stress, displacement and change of plasticity of the model in the surrounding of the excavation area as longwall advances.

The local high concentration of methane in goaf is studied through implementing computational fluid dynamics code FLUENT. The simulation results of FLUENT, will present information on distribution of velocity, pressure and mass fraction of methane in the goaf region. Furthermore, the results are analyzed identifying region of high accumulation of methane.

The simulation results of FLAC and Fluent are used as a basis to provide theoretical guidance of methane drainage in the region of overburden strata above goaf and in goaf. The parameters of the methane drainage using high-level and low-level drill holes will be arranged in accordance with overburden strata structure obtained by FLAC3D simulation. The installation of pipe will depend on location of high methane concentration, thus, on the results of FLUENT.

---

## 2 Location and general description

---

### 2.1 Location

---

Qianjiaying Mine is a subsidiary of Kailuan (Group) Co., Ltd. Most of Qianjiaying Minefield is located in Fengnan District, Tangshan City, Hebei Province. The mine field is located in the southeastern Tangshan City, Hebei Province as can be seen in Figure 2.1.

Geographical coordinates are:

East longitude: 118°14'12" ~ 118°24'43"

North latitude: 39°30'13" ~ 39°38'32"



**Figure 2.1 The location of Qianjiaying Coal Mine**

The mine is 14.5 km and 16 km respectively away from Tangshan station and Guye Station of the Jingshan Railway Station. The northeast and north of the minefield are adjacent to Fangezhuang Minefield and Lujiabang Minefield respectively. The mine has 5 recoverable coal seams in total among which the 5, 7, 8, 9, and 12 coal seams are main working seams. The current mining depth is at the level of -850 m.

---

### 2.2 Description of working face

---

The working face 2874W is located in the south of Miaozhuang village. The thickness of coal seam varies between 3-5.5 meters. Part of the coal seam, approximately 0.2 is placed between siltstone. There is a layer of unstable mudstone at the bottom of coal seam with approximate thickness 0-0.3 meters. The working face has relatively large slope gradient

with the inclination of coal seam varying from 6-24 ° and average inclination degree of 16°. The length along strike direction is 1342.7-1344.7 meters and average length along strike is considered 1343.7 meters. The length of coal seam along dip direction is 204.7 meters. The level of working face is approximately -692.3 to -813.8. The working face utilizes bidirectional (bi-di) coal cutting, where coal must be cut along the boundaries of plate, workface must cut at the same level or flat and large fluctuations are forbidden. Based on the thickness of coal seam, the mining height can be adjusted. The working face implements "U" type of ventilation is implemented as can be seen in the Figure 2.2.

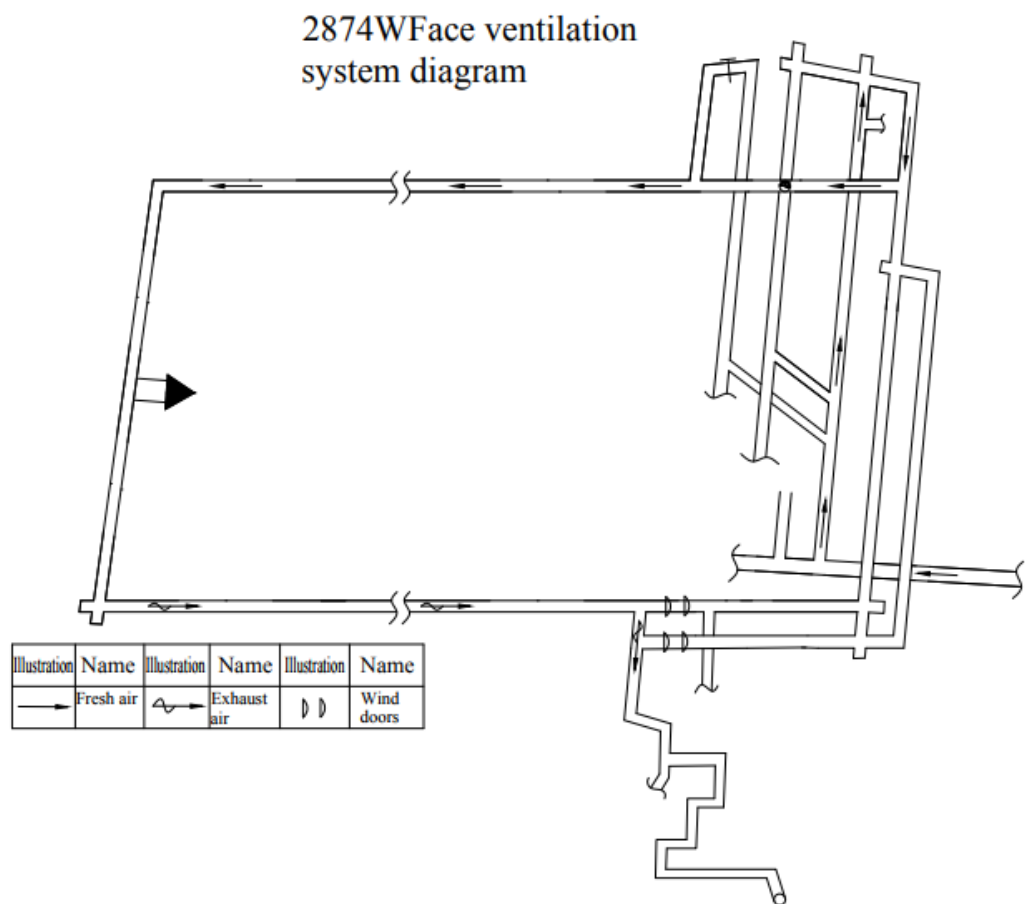


**Figure 2.2. The ventilation layout of the 2874 W working face**

---

## **2.3 Fault and folds**

There are few large and medium-sized faults and crosscuts in the mine field. A total number of 26 faults are identified and controlled. Among those faults, 6 faults have 30-50 m gaps, 7 faults have 10- 30 m gaps and less 10 faults have gaps less than 10 m. In addition, there is little change in the attitude of stratum, and there are few loose folds mainly including

synclines Bigezhuang, Xiaogezhang, and Gaogezhuang, saddle structure in Wanggezhuang, and anticline in Nanyangzhuang; The folds in the southwest include synclines Li Xinzhuang and Shengang as well as anticline Liutangbao. The monoclinic tectonic accounts for a large part of the mine range. The local section is affected by magmatic intrusion.

From the perspective of the entire coal field, stable coal seams (7#) and relatively stable coal seams (9, 12 #) accounted for 77.2% of the total field reserves.

In the early time of mining, working face 2874 west is influenced by f3, f4, and the 2874West f2, f5, f1, 8DF3, f6 and other faults, roof pressure together, resulted in fragmentation of coal rock strata and relatively poor stability

---

## **2.4 Mine gas sources**

---

Coal seam number 7 has content of relative gas emission rate of  $7.567 \text{ m}^3/\text{t}$  and the absolute gas emission rate is  $15.5 \text{ m}^3/\text{min}$ . Main gas source in Qianjiaying mine is mine shaft while the coal crushing process takes place. The proportion of gas emission from the recovery working face and tunneling working face respectively accounted for 60.71% and 22.46% compared to whole gas emission in the mine.

---

### 3 Simulation the response of overlying strata to longwall mining using FLAC3D

---

Longwall mining disturbs the initial stress equilibrium and rock mass deforms and caves down indicating that there exist some parts of the rock strata, which experience relative similarities both in nature and in degree of deformation damage stating that these parts are put together into zones when displacement schemes are being formed (Turchainov et. al., 1977).

---

#### 3.1 Formation of three zones

---

The overlying goaf area strata can be divided into "three zones" in vertical direction: caving zone, fractured zone and bent deformation zone; "three zones" in longitudinal and transverse directions: sustaining affect zone, separation zone and compaction zone as can be seen in Figure3.1. This division of zones is based on the extent of fractures in the overlying strata, scope of deformation damage, stress status as well as characteristics of degree of re-compaction and status of fissures to sustain the caving process (Zhang et. al., 2012).

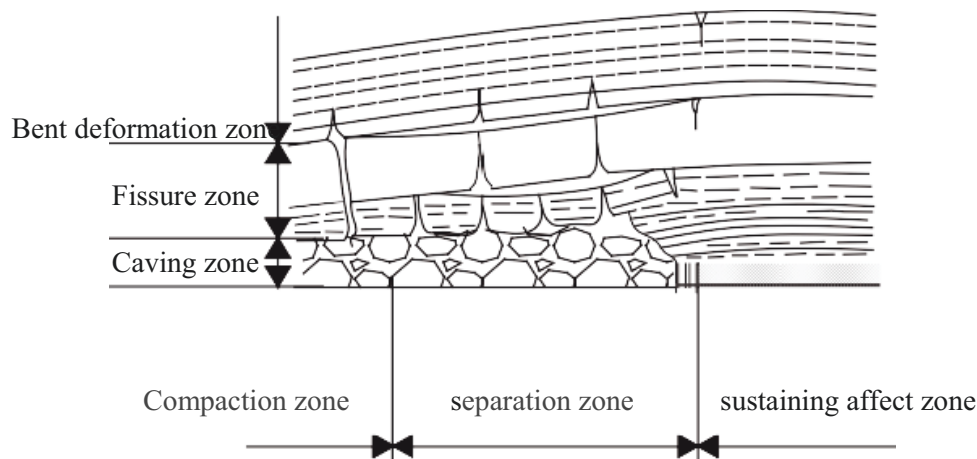


Figure 3.1. Division of three zones adopted from (Zhang et al., 2012).

Strata of the caving zone undergoes the process of deformation and caving with the rock mass of the immediate roof deforming, undergoing the process of separation of beds, breaking and eventually collapsing down, accumulating on the mine floor. Thus, forming a region of unevenly broken parts of overburden strata distinctive in its characteristic of having large amount of pores among the rock blocks with various shapes and sizes creating irregular fractures in this region that have good connectivity (Zhang et al., 2012; Palchik, 2003).

Even though gas in the goaf area of the caving zone has relatively high distribution, the concentration of it in that zone is relatively low due to the flushing of air from ventilation (Tian-xuan, Zhi-chao and Feng, 2012; Qu et al., 2015).

The caving zone is distinct in having both vertical and horizontal fractures. The maximum height of caving zone can be estimated by using formula 3.1

The maximal height of the caving zone is calculated using the formula (3.1) below:

$$a = \frac{h}{(K_p - 1) \cos \alpha} \quad (3.1)$$

where a-the height of caving zone, m. h-mining height of coal seam, m.  $K_p$ -bulking coefficient of caved rock;  $\alpha$ -the dip angle of coal seam, ( $^\circ$ ).

The zone located above the caved zone is fractured zone. The fracture channels within the fractured zone connect zones bent deformation zone and caving zones (Zhang et al., 2012). Table 3.1 displays empirical measures of determination of the height of the fractured zone widely used in China.

Strength rank of overlying strata	Height of the fractured zone (m)
Strong	$H_d = \frac{100\sum M}{1.2\sum M + 2.0} \pm 8.9$
Medium strong	$H_d = \frac{100\sum M}{1.6\sum M + 3.6} \pm 5.6$
Weak	$H_d = \frac{100\sum M}{3.1\sum M + 5.0} \pm 4.0$
Very weak	$H_d = \frac{100\sum M}{5\sum M + 8.0} \pm 3.0$

**Table 3.1. Empirical expressions between height of the overlying fractured zone ( $H_d$ ) and the mining thickness (M) used in China**

Adopted from (Du and Wang, 2003) in (Qu et al., 2015).

The fractured zone can be subdivided into three parts, namely: zone of rock blocks, directly above it is zone with through-going vertical fractures and upper part of fractured zone mostly formed with horizontal fractures. The lower part of the fractured zone is characterized with formation of vertical and horizontal fractures. Middle part of fractured zone is also characterized with formation of horizontal fractures due to bed separation, while

number of through-going vertical fractures in the middle part is considerable less than that in lower part of fractured zone. In upper part of fractured zone only horizontal fractures occur and there are not vertical fractures present in the region due to the overlying strata thickness (Palchik, 2002).

The lower part of the fractured zone is more suitable for gas migration and storage compared to upper part of fractured zone. Due to formation of vertical fractures that are connected to horizontal fractures induced by bed separation, gas is able to migrate and to accumulate in relatively high concentrations in the lower part of the fractured zone. The upper part, on the other hand, can store little amount of high goaf gas concentration as a result of development of bed separated fractures (Tian-xuan, Zhi-chao and Feng, 2012).

The fractures in fracture zone experience development, adequate development and compression. Fractured zone is most developed in the separation zone (Figure 3.1). The formation of fractures enhances the permeability, creating path ways for gas to accumulate and release to (Zhang et al., 2012).

The methane in the fractured zone is able to be desorbed to some degree owing it to the de-stressing, with the gas mainly flowing in the horizontal direction. Due to re-compaction of goaf and associated with it recovery of pressure, once desorbed methane is able to re-adsorb again if not drained (Qu et al., 2015).

The zone overlying the fractured zone is continuous deformation zone, which is also known as bent zone or bent subsidence zone. The strata of this zone does not experience fissuring or de-stressing and hence why the methane in this zone keeps in the adsorbed state in coal matrix (Qu et al.,2015).

---

## **3.2 Stress zones division**

---

Along with division of three zones, the overlying strata above goaf, can be divided into four zones longitudinally according to characteristics of stress. The division of these zones are recompaction zone, strata separation zone, stress abutment zone and zone with initial stress, as is illustrated in Figure 3.2. With the advancing of the working face, the overlying strata undergoes process of increase of stress from original stress to abutment pressure, following the decrease of stress and then recovery of stress. Consequently, the roof

will undergo stages of compression related to increase of stress, tensile deformation associated with the stress relief followed by recompression (Meng et al., 2016).

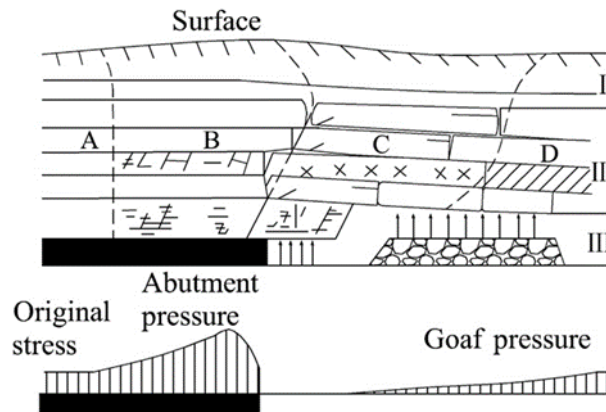


Figure 3.2. The failure and deformation experienced in overlying strata during longwall mining adopted from (Meng et al., 2016).

### 3.3 The relationship between permeability and fracture

Deformation significant alteration in permeability with related to formation network of fissures with good connectivity.

The permeability fracture relationship:

$$k_l = \frac{w_f^2}{12} \cdot \phi_f \quad (3.2)$$

Where  $k_l$  is the permeability (mD);  $\phi_f$  is fracture porosity (decimal);  $w_f$  is the fracture aperture (mm)

Thus the greater the fracture aperture, the greater the value of permeability.

According to (Rowland et al., 2008) the permeability is related to the development of fractures. (Laubach et al., 1998) found out that in a system connectivity of fissures as well as network geometry are essential to augmentation of permeability that fissures can contribute.

Moreover, the experimental research by (Cai et al., 2014) concludes that the connectivity of fissures have more significant impact on permeability than having biggest area of fissure development.

Being one of the most crucial factors affecting the migration and gas release, permeability is dependent on development of fissures in the caved and fractured zones (Qin et al., 2015).



The conclusion that permeability value will increase with the amount of generated fractures can be made.

---

### **3.4 Simulation by FLAC3D**

---

FLAC3D (Fast Lagrangian Analysis of Continua in 3 Dimensions) is a three-dimensional explicit finite-difference software implemented for solving engineering mechanics computation problems. In this research paper, based on the geological conditions of Qianjiaying coal mine, FLAC3D software was implemented for numerical simulation analysis of fracture generation in the overlying coal seam 7 strata. The research aim is investigated by analyzing the change of displacement, stress and plasticity of the model as excavation proceeds.

---

#### **3.4.1 Geometry of the model**

---

The size of the whole model is 400m (length)×600m(width)× 237.17(height). The dip angle of rock and coal seams is 16°. The x-direction is the incline direction, the y-direction is the strike direction and z-direction is the direction of gravity of the coal seam as is shown in the (Figure 3.3). The model is divided to 9 layers in order to fully replicate the conditions under which coal seam is being mined. The relevant input data for simulation model was taken from the geological prospecting report of Qianjiaying coal mine and can be seen in the Table 3.2.

Layer number	Lithology	Thickness (m)	Inclination (°)	Accumulative thickness
1	Mudstone	30	16	102.67
2	Siltstone	14	16	72.67
3	Fine-grained sandstone	20.74	16	58.67
4	Coal seam 6	0.35	16	37.93
5	Mudstone	3.82	16	37.58
6	Coal seam 7 (working )	4.26	16	33.76
7	Siltstone	7.3	16	29.5
8	Coal seam 8	2.2	16	22.2
9	Mudstone	20	16	20

**Table 3.2. Input data for simulation**

### **3.4.2 Description of the model**

A preliminary grid model was established and solved in order to generate the response of overlying strata to the proceeding excavation of coal through analysis of the stress, displacement and element state of the model. The model was established using brick-shaped mesh to simulate field situation.

Empty unit excavation mode was implemented to simulate the advance of working face. Every time when the working face advances to 20 m of excavation meaning emptying of 20 m of the model, the calculation step was set to 2000. A three-dimensional model with a total height of 217.37 m was established. The width of barrier pillar is chosen to be 100 m. The model will gradually excavate from  $x=100$  m until excavation  $x=300$ m. The initial stress distribution of the model in vertical and horizontal directions is shown in Figures 3.4 and 3.5.

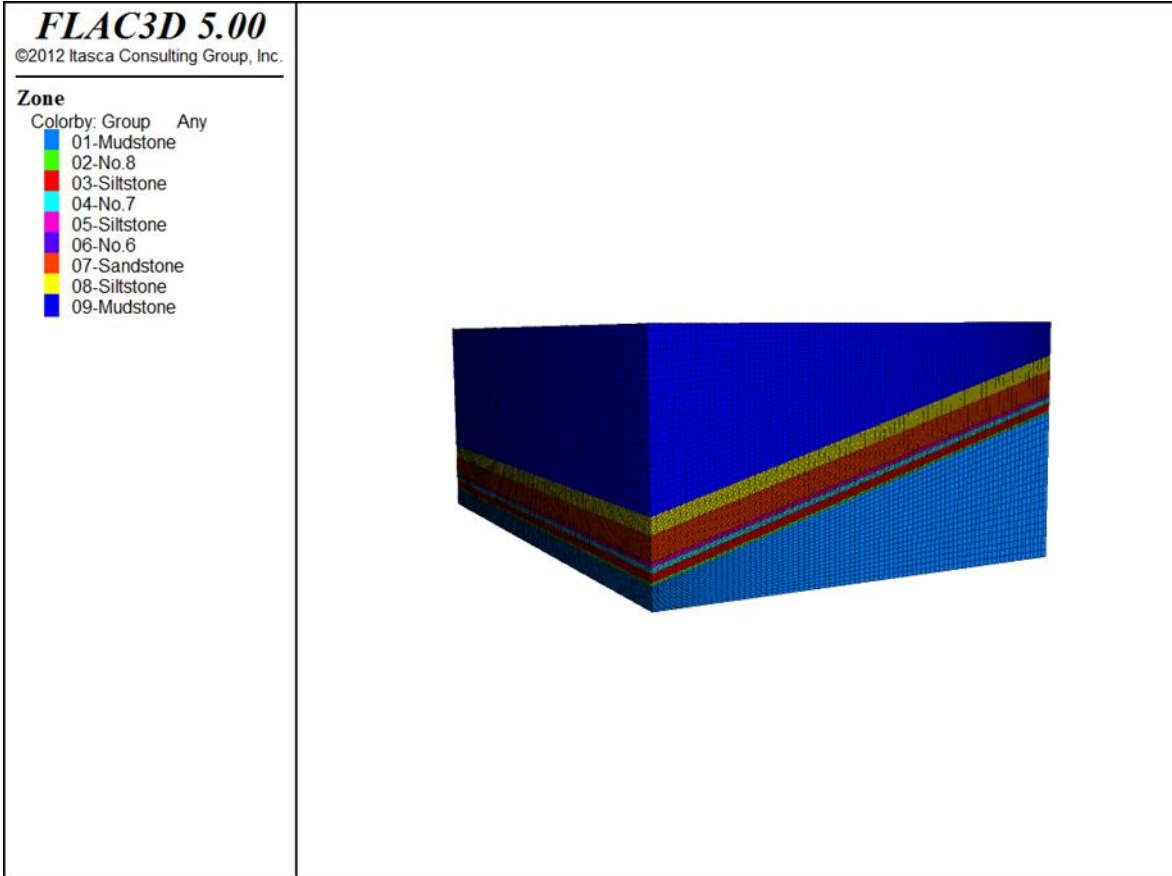


Figure 3.3. Numerical simulation model

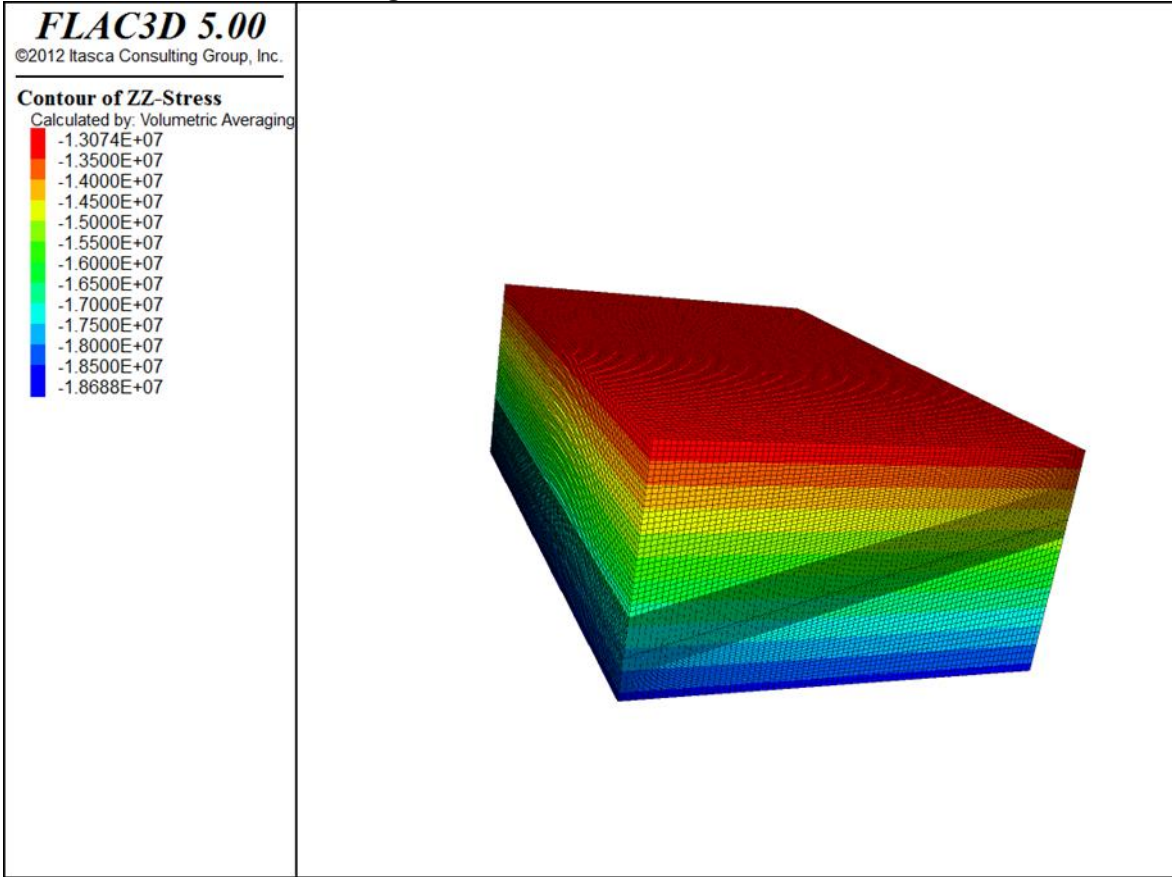


Figure 3.4. Initial vertical stress distribution

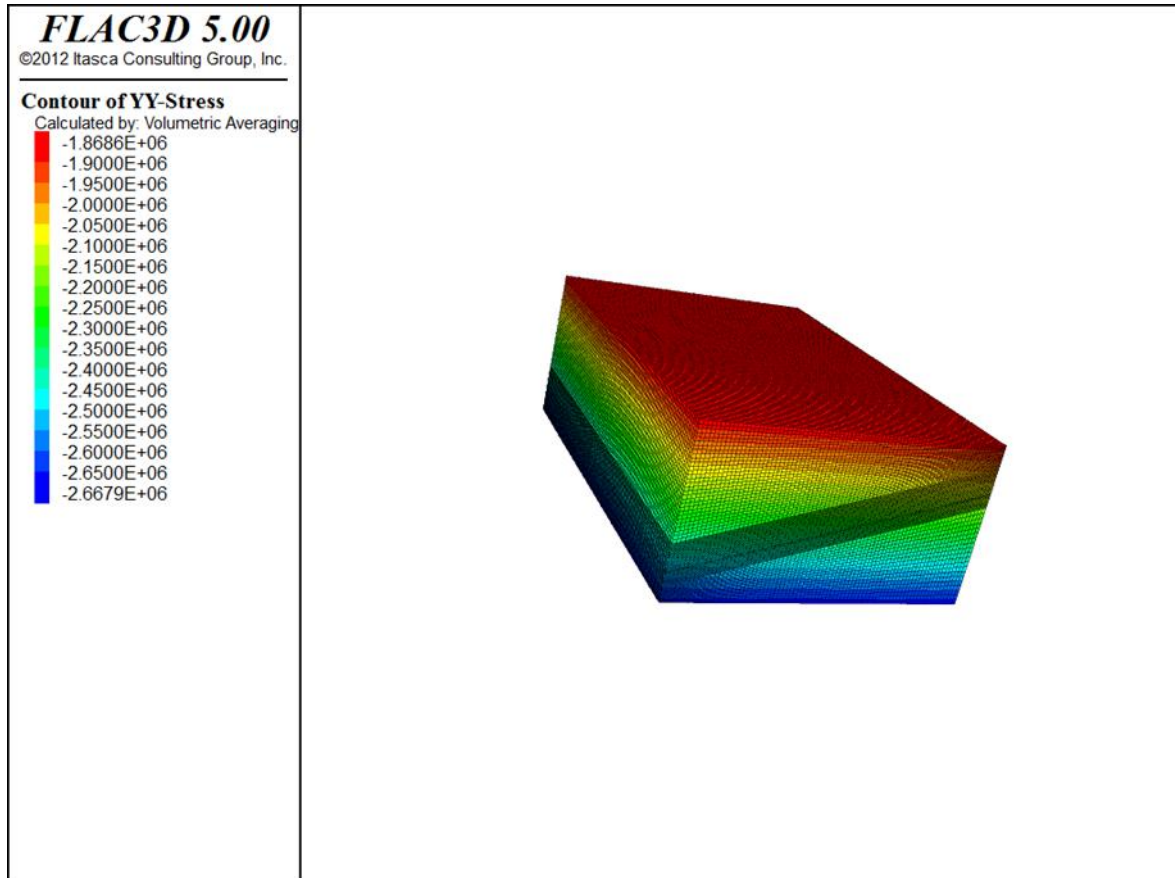


Figure 3.5. Initial distribution of horizontal stresses

### 3.4.3 Boundary conditions and parameters

In this simulation the boundary conditions around the model are fixed at the bottom of the model, but the upper part is not fixed. In order to determine the deformation of the rock mass in the model, the Mohr-Coloumb criterion was used.

Stress boundary(S-B) method was used in order to simulate the initial stress field. There is no boundary of force, which is realized by redistribution of stresses in the model. Vertical and horizontal stresses with the magnitudes of 18.93MPa and 9MPa respectfully were applied on the direct roof of coal seam. The basic parameters used to perform simulation are listed in the Table 3.3.

Strata index	Cohesion (MPa)	Shear Modulus (GPa)	Bulk modulus (GPa)	Apparent density (kg/m <sup>3</sup> )	Tensile strength (MPa)	Internal friction angle (°)
Overlying stone (Mudstone)	6.67	4.0	6.67	2160	9.7	32.1
Siltstone	10.83	8.13	10.83	2460	1.84	38
Fine grain sandstone	16.04	12.02	16.04	2800	4.96	43
Coal seam 6	1.67	1.36	1.67	1460	2.3	27.8
Mudstone	9.97	7.35	9.97	2483	0.58	32
Coal seam 7	1.67	1.36	1.67	1460	2.3	27.8
Siltstone	10.83	8.13	10.83	2460	1.84	38
Coal seam 8	1.67	1.36	1.67	1460	2.3	27.8
Underlying stone (Mudstone)	6.67	4.0	6.67	2160	9.7	32.1

**Table 3.3. Mechanical and physical properties of the model**

## **3.5 Results**

### **3.5.1 Vertical stress distribution**

The original stress equilibrium state of coal seam 7 was destroyed due to extraction of coal. The newly formed opening underground causes the original stress to redistribute over surrounding rock strata forming new stress state around stope. The redistribution of stress is continuing process changing every time as mining face advances. The development

of vertical stress in both dip and strike direction of the coal seam each 20, 100 and 200 meters of working face advance is presented in Figures 3.6-3.11.

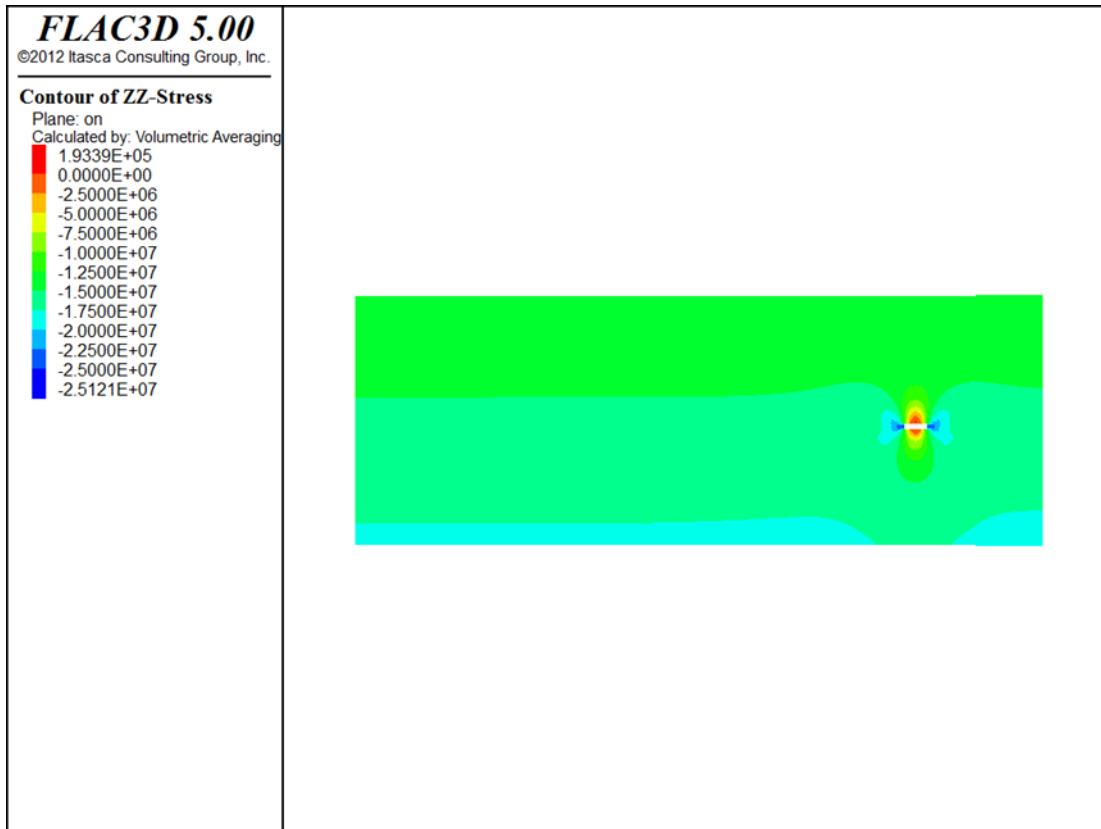


Figure 3.6. The vertical stress profile of the model along direction of strike after mining out 20m

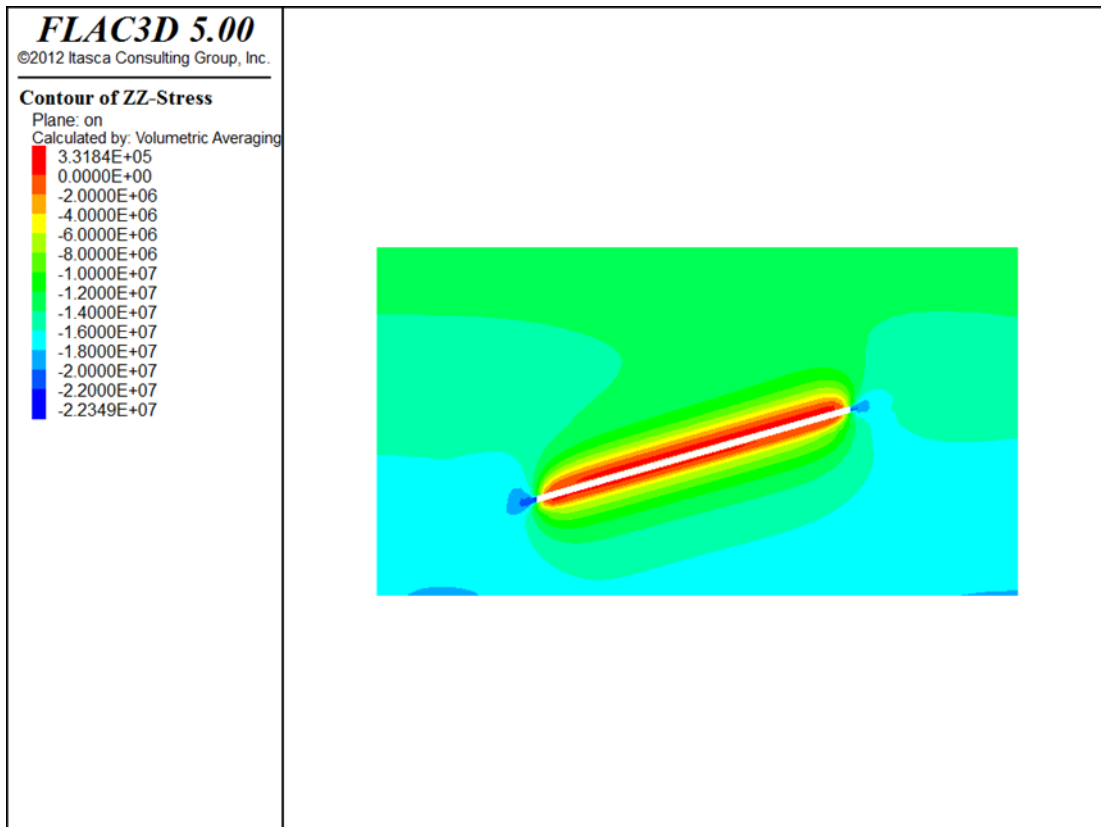


Figure 3.7. The vertical stress profile of the model along direction of the dip after mining out 20m

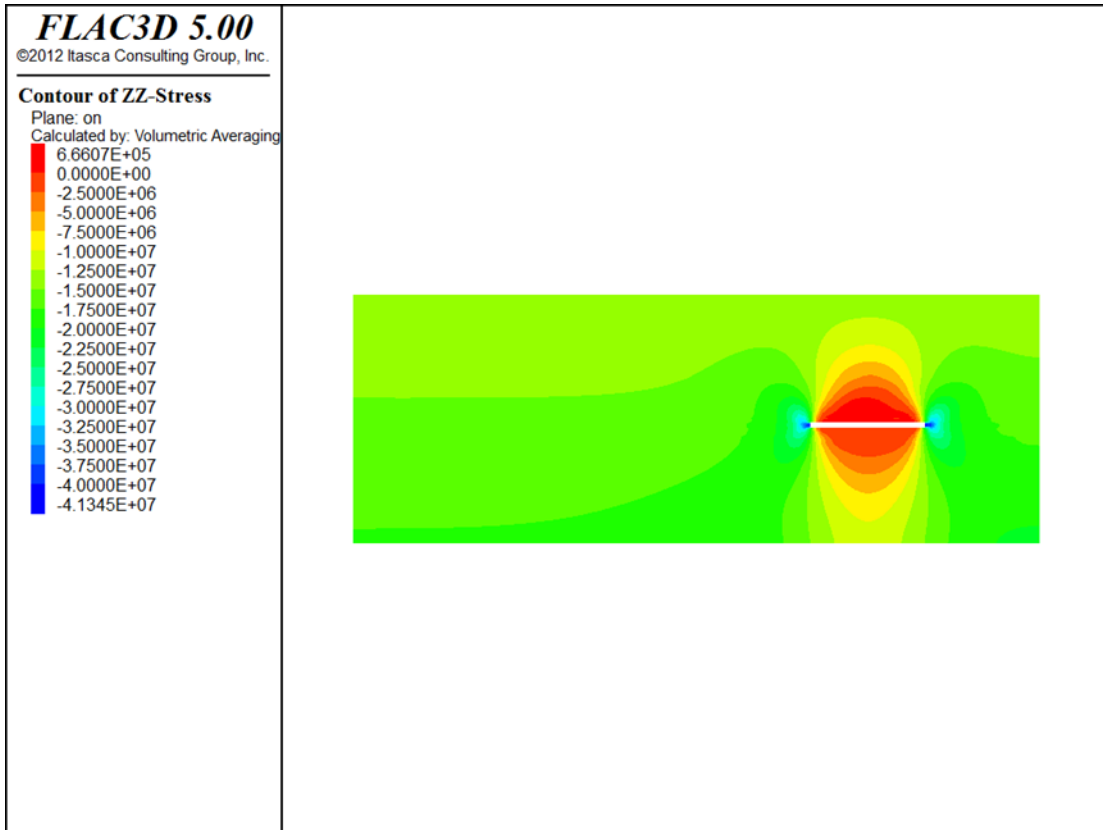


Figure 3.8. The vertical stress profile of the model along strike direction after mining out 100 m

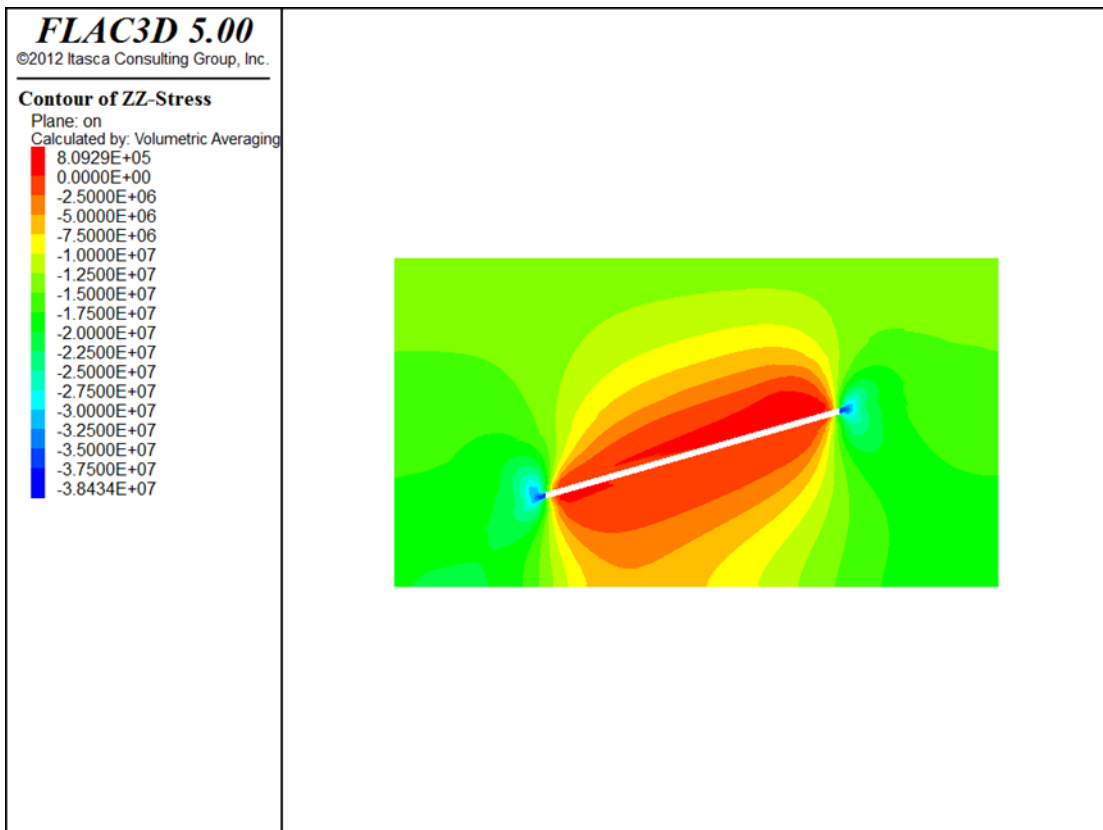


Figure 3.9. The vertical stress profile of the model along the dip direction after mining out 100 m

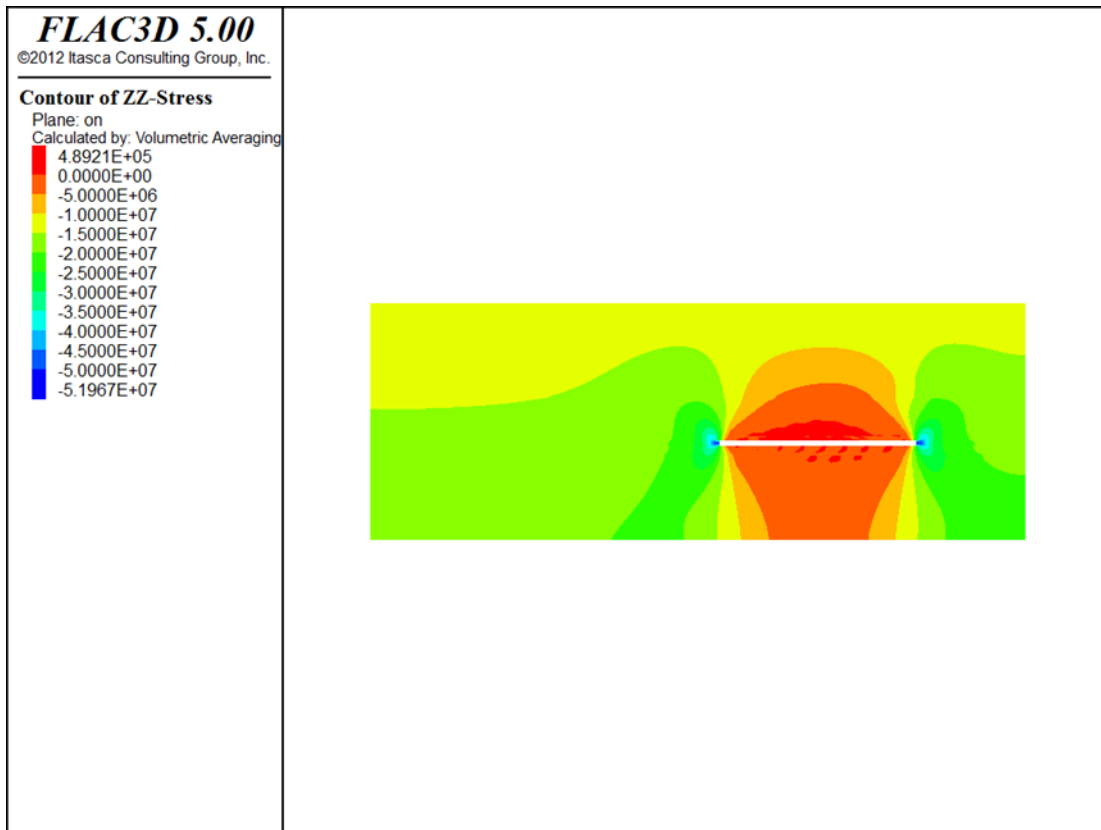


Figure 3.10. The vertical stress profile of the model along direction of strike after mining out 200m

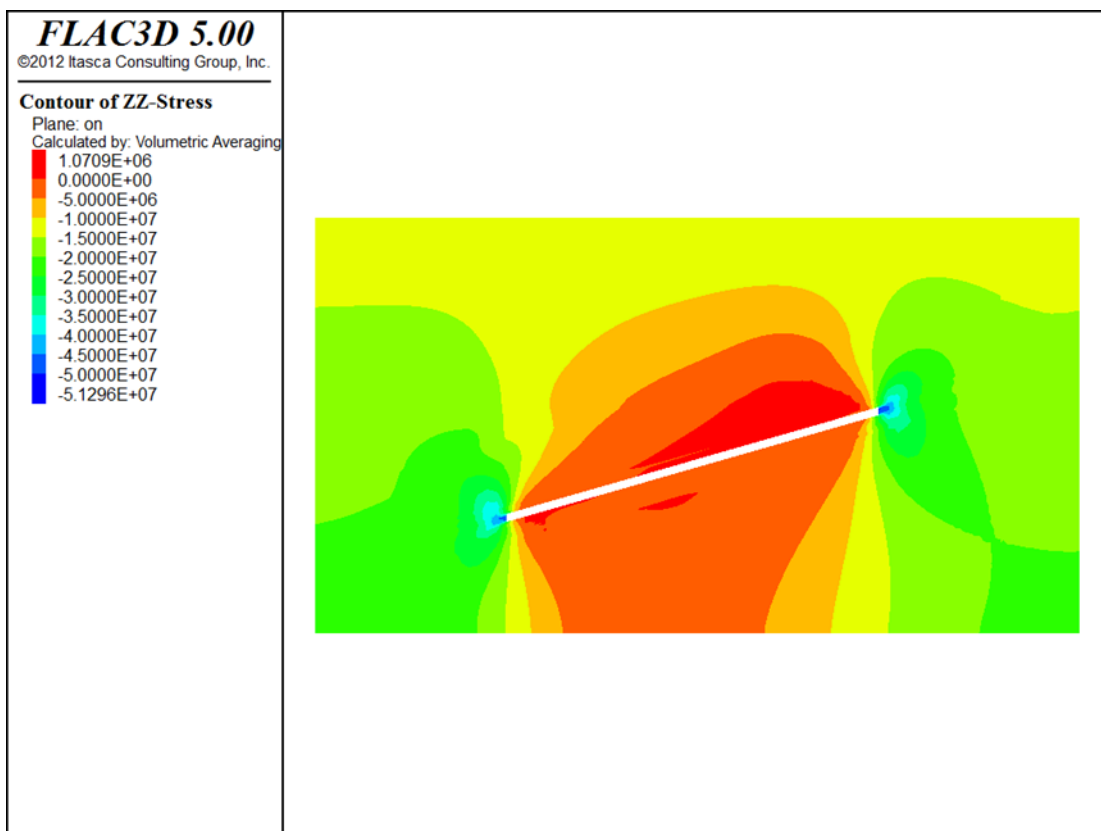


Figure 3.11. The vertical stress profile of the model along the dip direction after mining out 200m



From observing the results of simulation, it can be concluded that with the advancing of working face, the vertical stress distribution area increases. Whilst extraction of coal takes place, the overlying the stope strata will experience tension while the either side of excavation-compression. There also can be observed formation of stress in tension on the floor of the excavated area suggesting that fractures will also be formed in the floor as well.

Analyzing the results of simulation of vertical stress development as working face advances, it can be concluded that owing it to the newly formed cavity associated with extraction of coal, positive stress is formed that is acting to the surface and due to the overlying rock mass pressure acting towards the cavity negative stress is formed.

The vertical stress is observed to have a trend of being smaller in the central part of mined out area immediately above extracted coal ( $8.0929 \cdot 10^5$  Mpa) and larger on the overlying strata area ( $-2.5 \cdot 10^6$  MPa) shown in Figure 3.9. This can be explained due to the impact of extraction of coal as the overlying strata caves down the stress redistributes forming the areas of larger stress-induced areas in the outer part of overlying rock mass.

Furthermore, there exist some areas formed on either side of excavation known as stress concentration areas. As overlying strata is collapsing, stress undergoes redistribution, but existence of cracks on either side of excavation formed due to extraction of coal, the stress cannot fully redistribute through this areas and localized build of stress concentration areas are formed on either side of the mined-out area.

Another conclusion from analyzing simulation results can be made related to the formation of vertical stress in the overlying strata: negative stress zone ( $-5 \cdot 10^6$  MPa) followed by zone with neutral stress (0) and central part above stope with positive vertical stress ( $1.0709 \cdot 10^6$  MPa) as can be seen in Figure 3.11. The counter acting of two stresses negative and positive will be the primary cause of generation of cracks in the overlying strata. The neutral stress zone is the zone of fracture formation.

Even though the vertical stress value in the middle part immediately above stope gradually decreased from  $6.66 \cdot 10^5$  MPa after excavating 100 meters (Figure 3.8) reducing to value  $4.89 \cdot 10^5$  MPa after excavation of 200 meters took place (Figure 3.10), the decrease of vertical stress does not signify the stress relief because of the possibility of the immediate roof to cave down at that excavation step. In this research paper, the area immediately above the stope will be regarded as caving zone. Furthermore, to prove the point the immediate roof above coal seam №7 is comprised of soft and not consolidated mudstone, it is

anticipated that it will cave down immediately after hydraulic support moves forward with advancement of working face.

With the advancement of working face, stress is expected to relieve in front of the working face.

---

### 3.5.2 Vertical displacement

---

The relief of pressure because of excavation of coal seam number 7 resulted in deformation and change in the vertical displacement in the overlying strata and surrounding rock of mined-out seam. The results of the simulation can be observed in Figures 3.12-3.17.

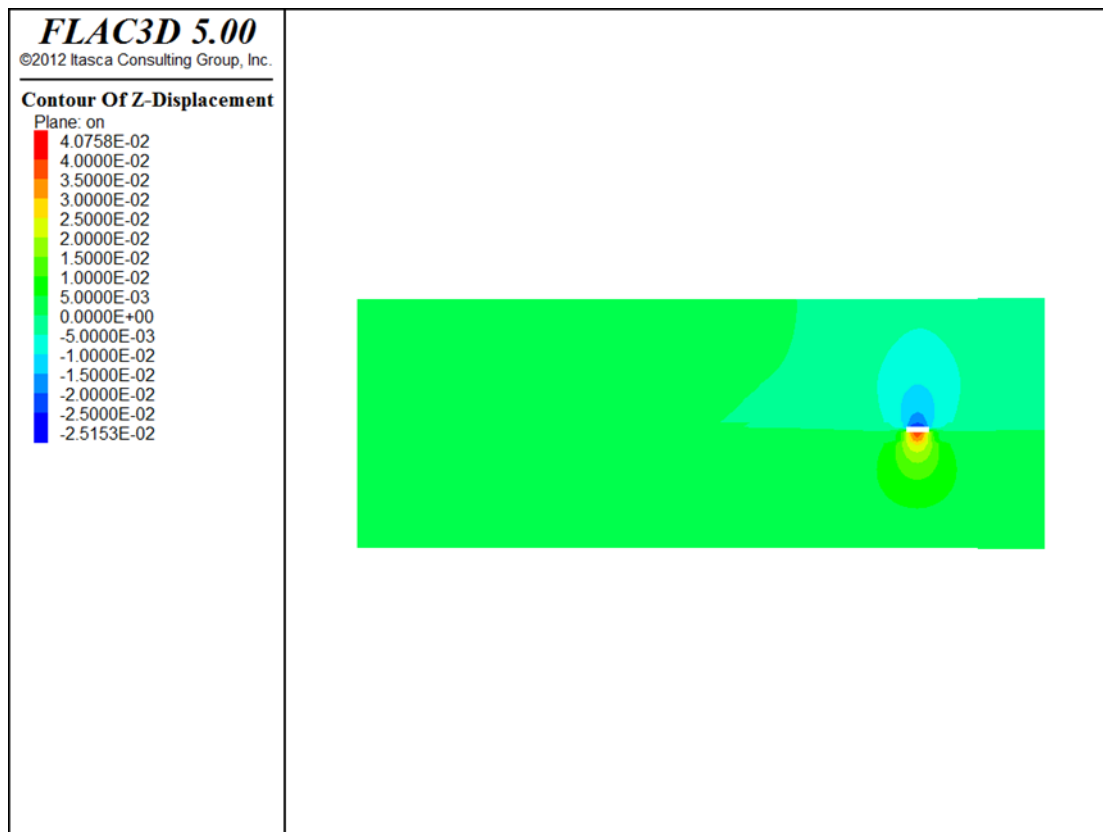


Figure 3.12. Vertical displacement of the model along strike direction after mining out 20m

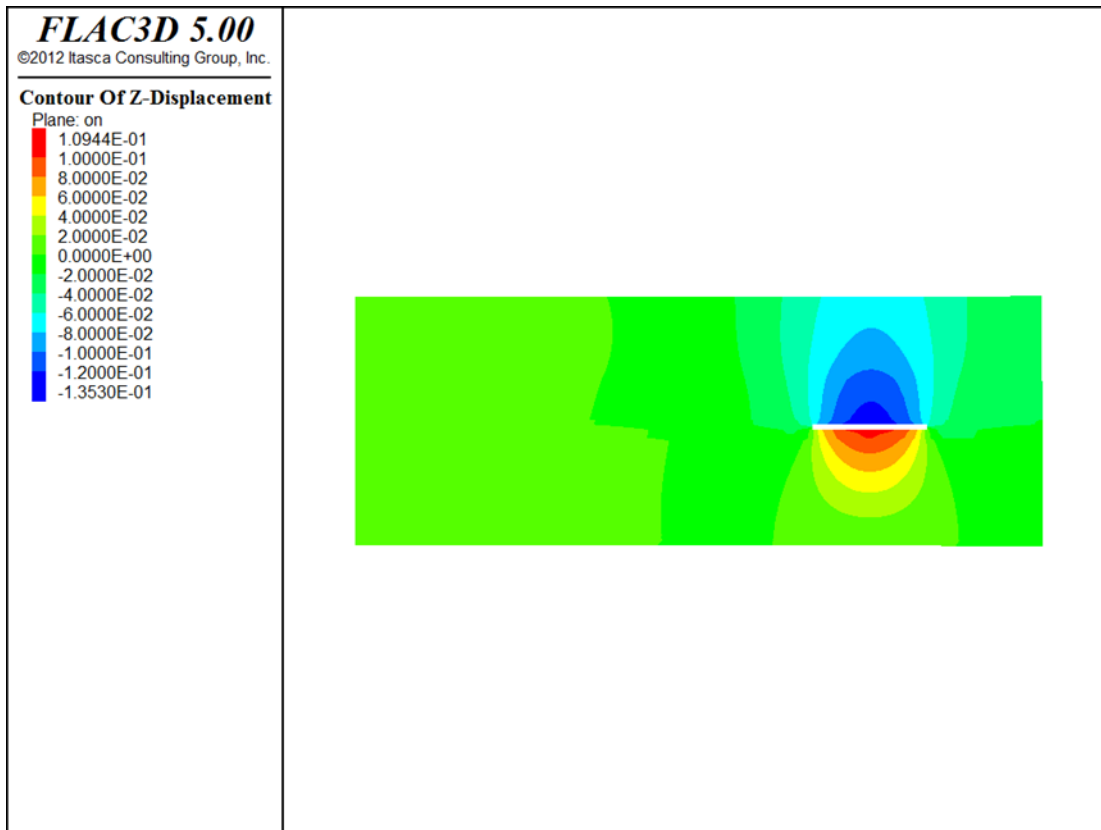


Figure 3.13. Vertical displacement profile of the model along strike direction after extracting 100 m

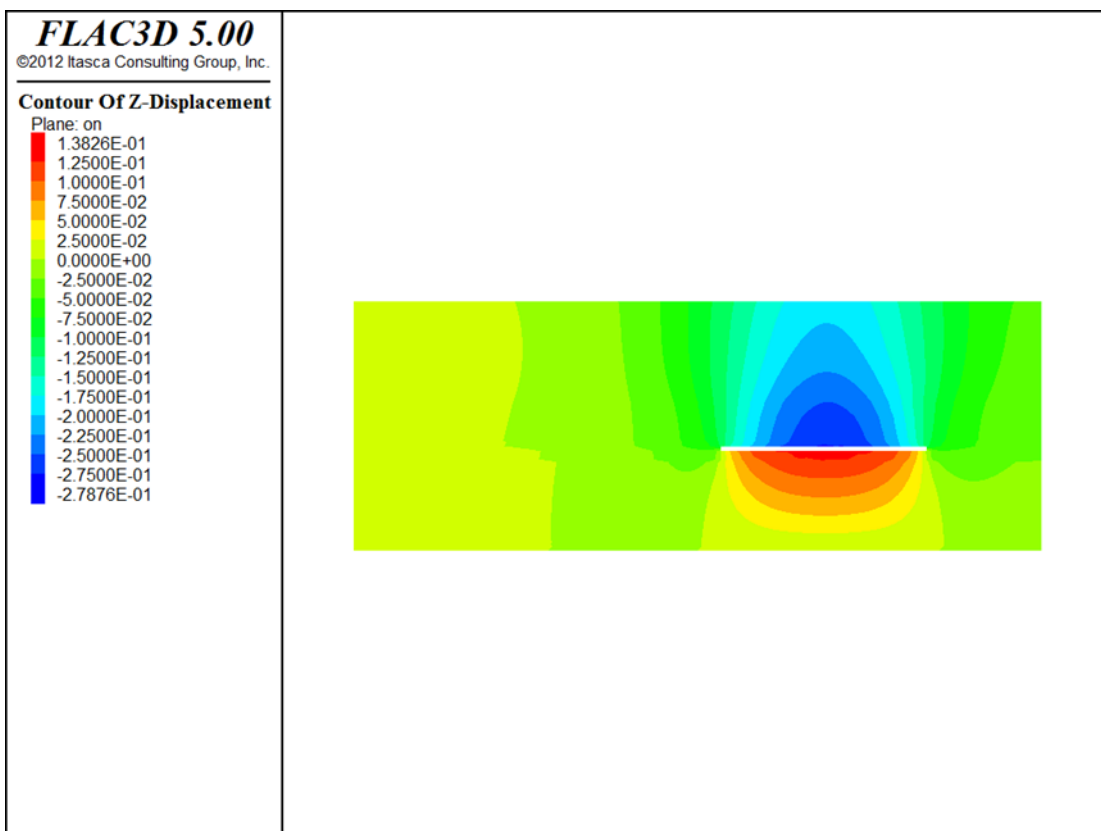


Figure 3.14. Profile of vertical displacement the model along strike direction after mining out 200m

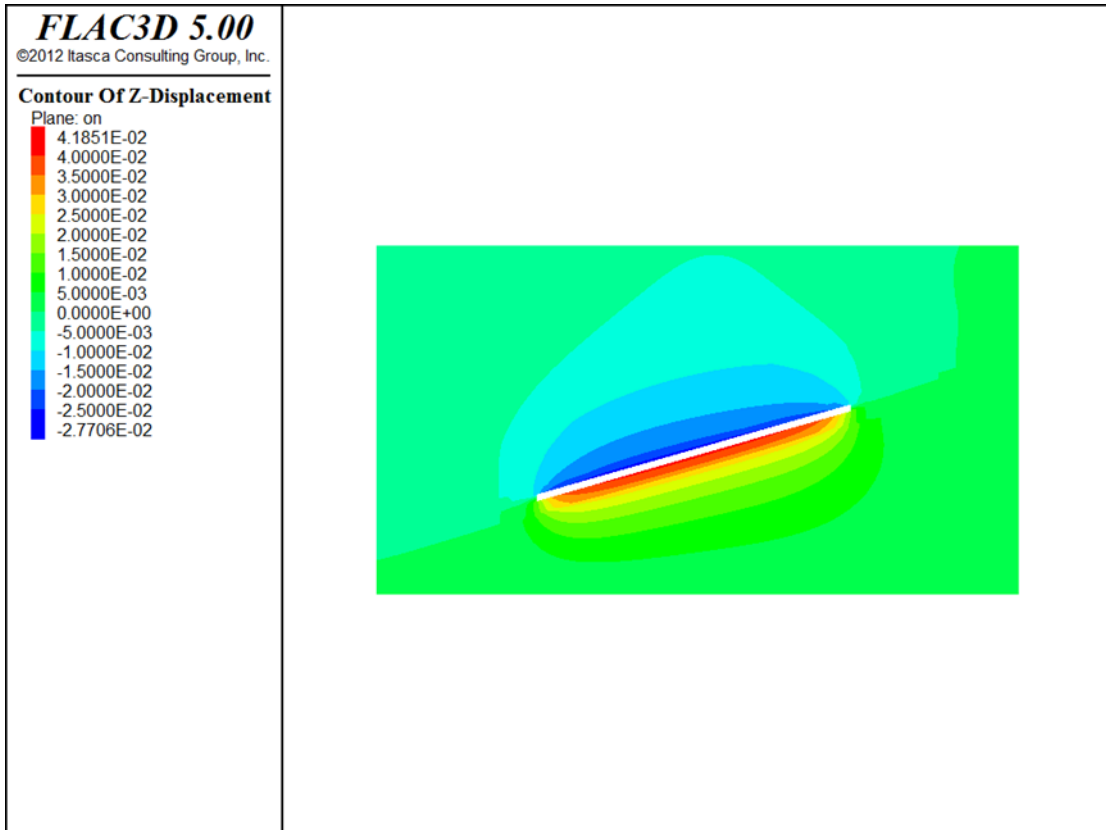


Figure 3.15. Profile of vertical displacement along dip direction after mining out 20 m

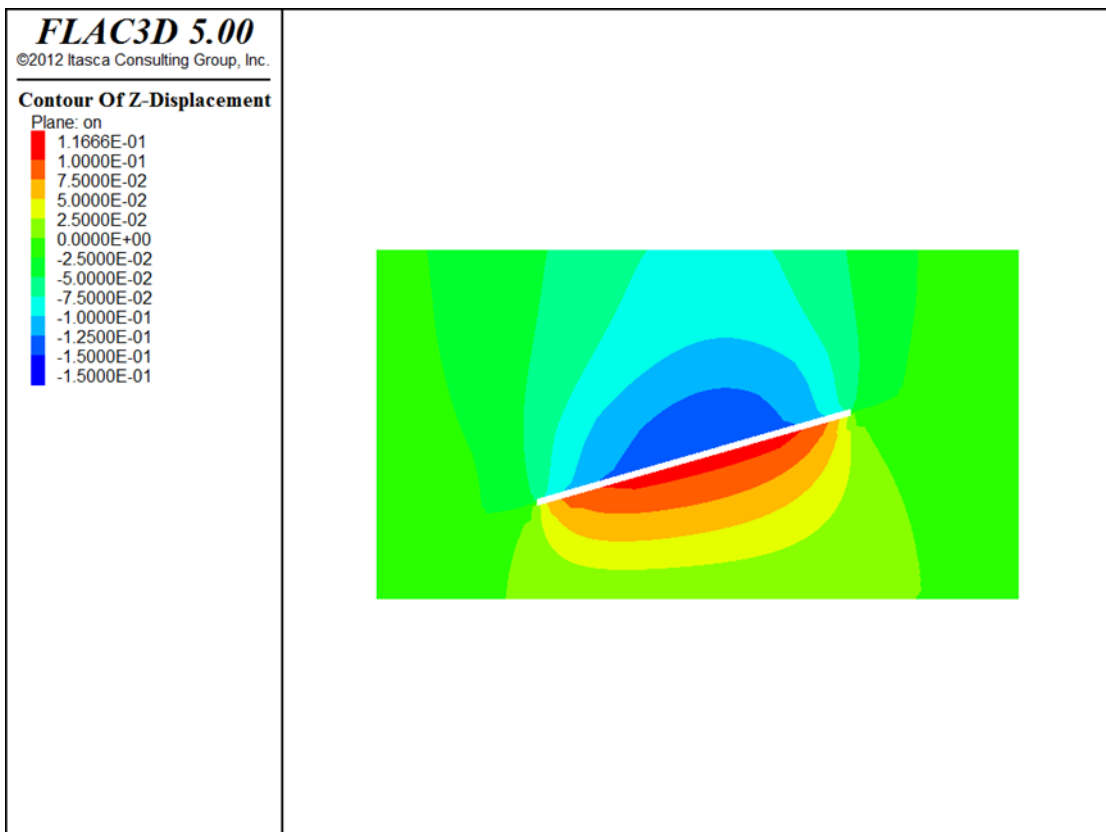
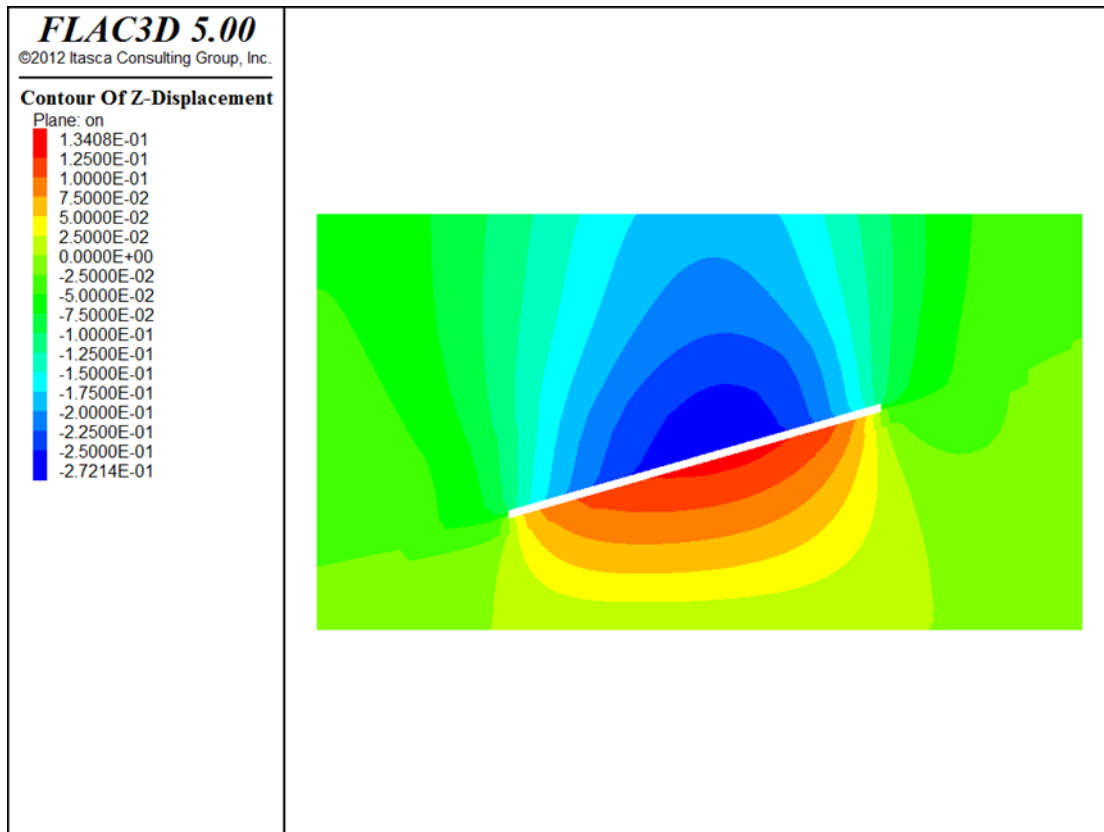


Figure 3.16. Profile of vertical displacement of model along dip direction after mining out 100 m



**Figure 3.17. Profile of vertical displacement of model along dip direction after mining out 200 m**

Due to the impact of mining, three distinct zones originated in the vertical direction: caving zone, fractured zone and bending subsidence zone. From observing the results of simulation, the displacement is formed in the arch-shaped form. The lower two arches formed immediately above the mined-out area represent the approximate boundaries of fractured and caved zones.

The values of vertical displacements increase with the advancement of the working face which indicate the larger scope of fractured zone as advancing of the working face proceeds. With the advancement of working face to 20,100 and 200m, the change in displacement was 0.015m, 0.1 m and 0.225 m accordingly (Figures 3.15; 3.16 and 3.17).

Owing it to excavation of coal, the pressure relief will be greater consequently resulting in generation of vaster area of fractured zone as working face advances.

As can be observed from figures 3.12-3.17, displacement immediately below excavation area is positive owing it to the force of expansion caused by creation of open space due to excavation of coal. On the contrary, the negative displacement occurring above the mined-out area is the result of overlying pressure of rock mass exerting force due to its

mass, which is significantly larger than the positive pressure exerted by open space in excavation being the reason for caving down of rock mass above mined-out area.

The fractures generated due to advance of working face to 200 m are considered to be stable because of degree of compaction.

Due to longwall mining, the strata above extracted area is allowed to fall down into the opening where coal used to be, creating relaxation of roof strata and subsequent generation of fissures.

---

### 3.5.3 Plastic damage state of the model

---

The rock mass is assumed to be elasto-plastic material. In order to analyze deformation state of the overlying strata, the changes in the plastic zone distribution in the overburden strata were analyzed. The changes in plastic element state of the model as excavation takes place 20,100 and 200 meters along directions of dip and strike can be observed from figures 3.18-3.23.

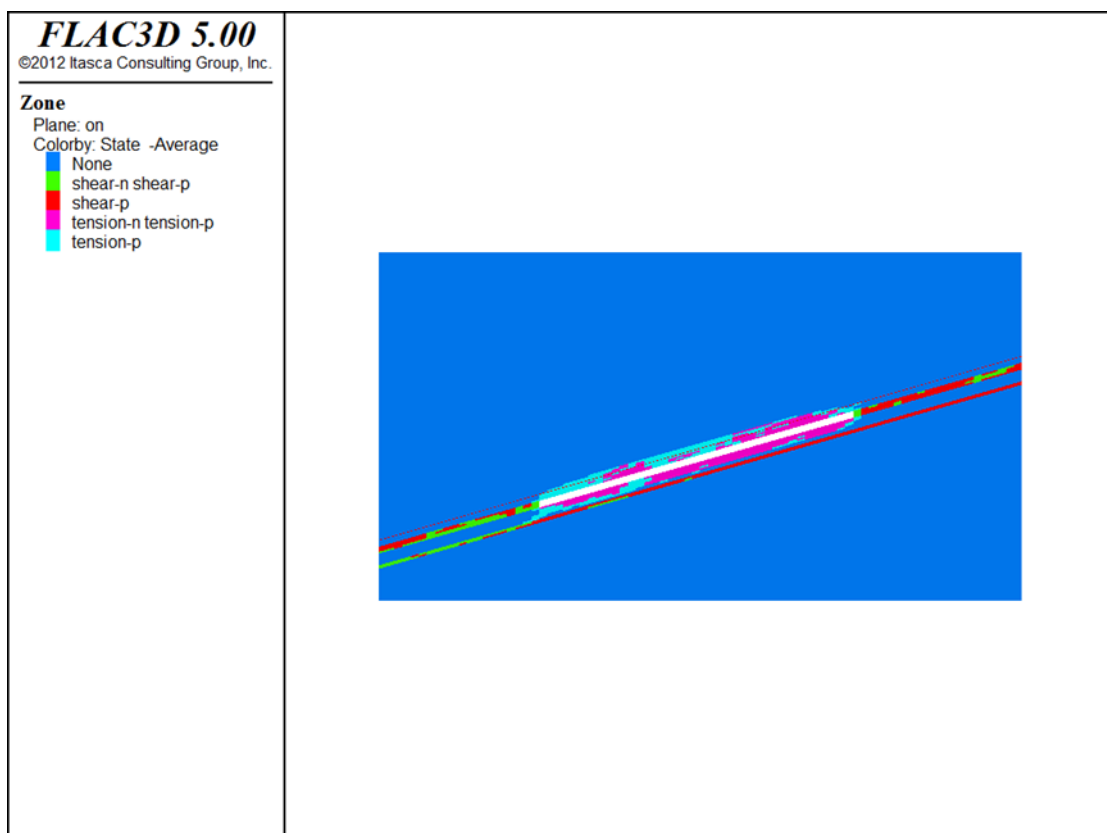


Figure 3.18. The model of damage state of the surrounding strata after mining out 20 m

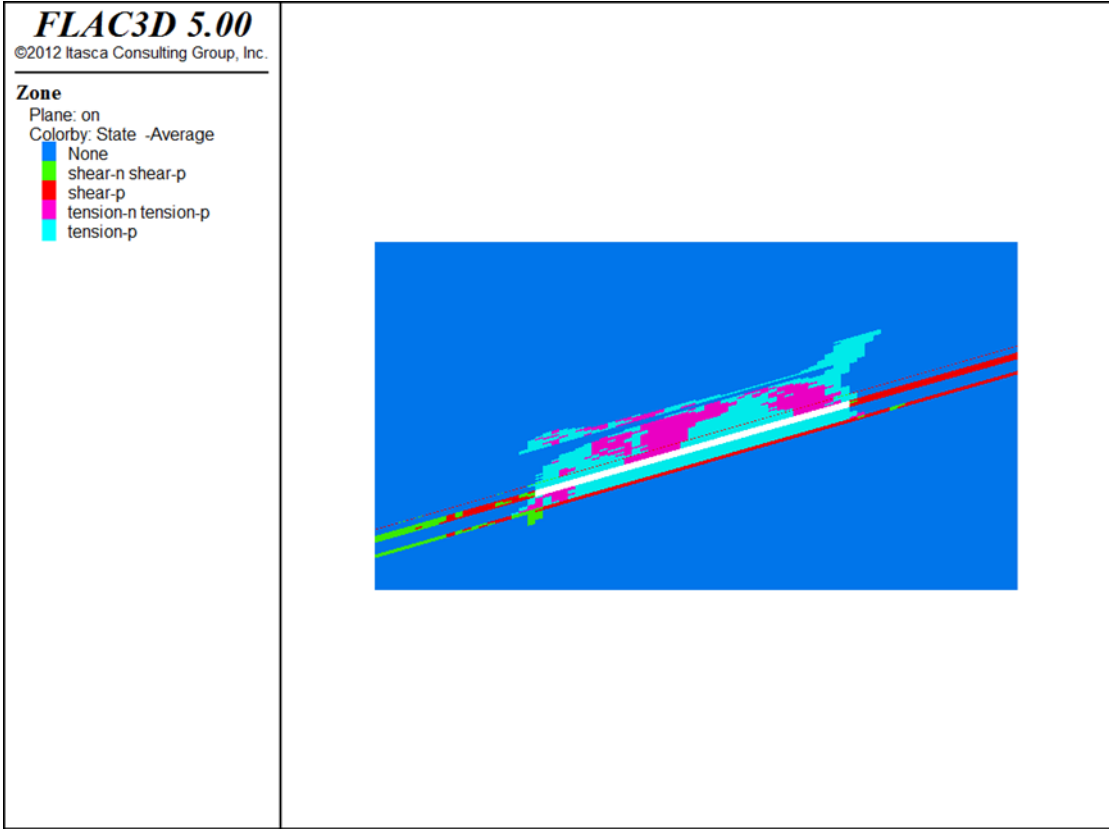


Figure 3.19. The model of damage state of the surrounding strata after mining out 100 m

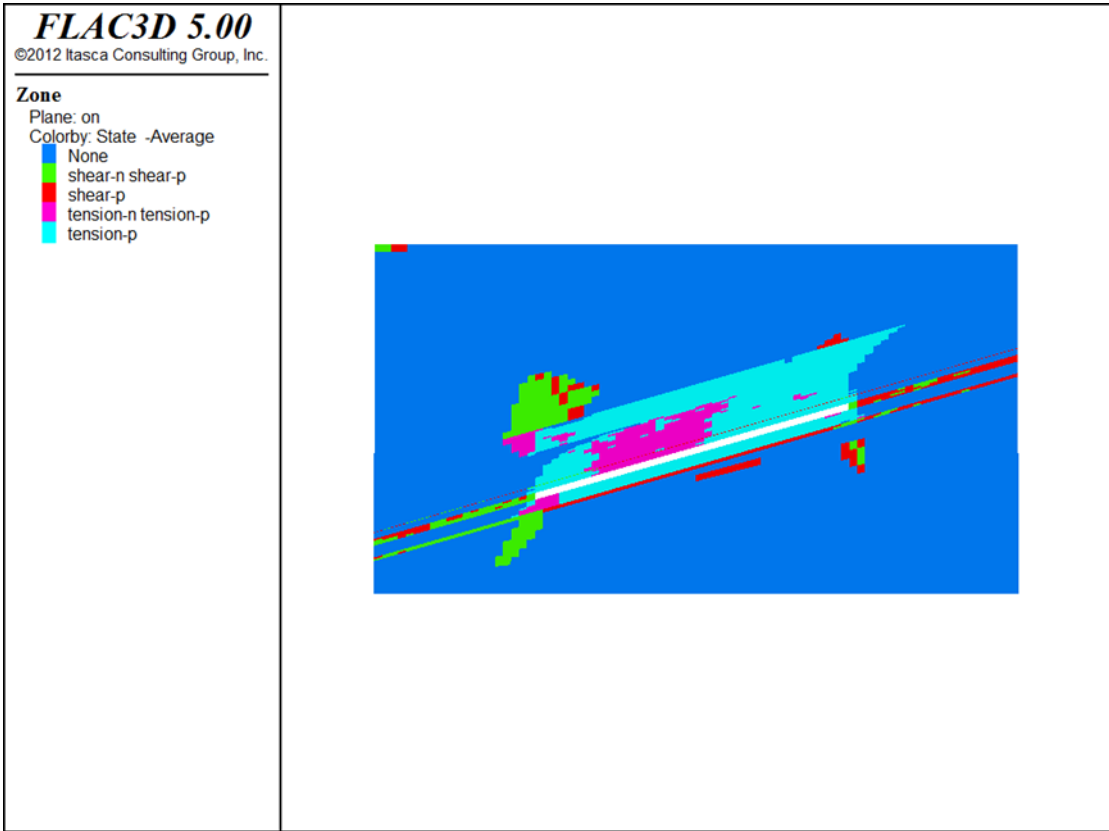


Figure 3.20. The damage state of the surrounding strata along dip direction after mining out 200 m

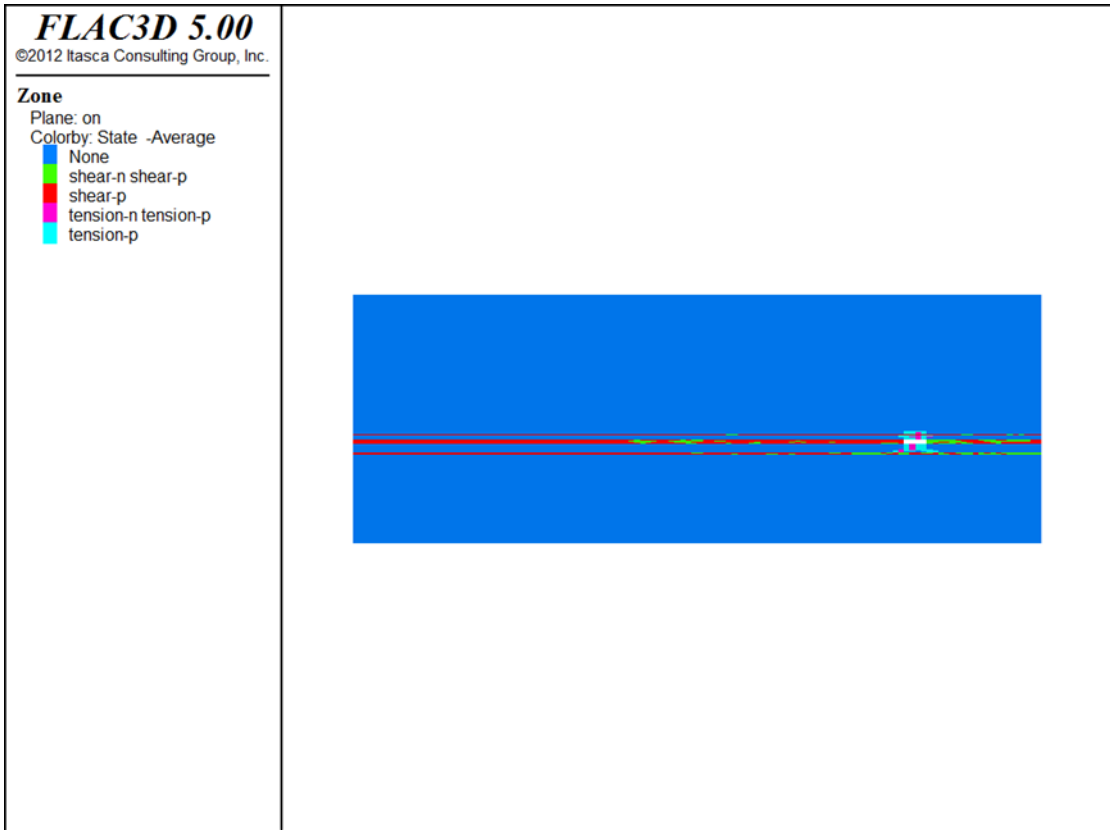


Figure 3.21. The damage state of the surrounding strata along strike direction after mining out 20m

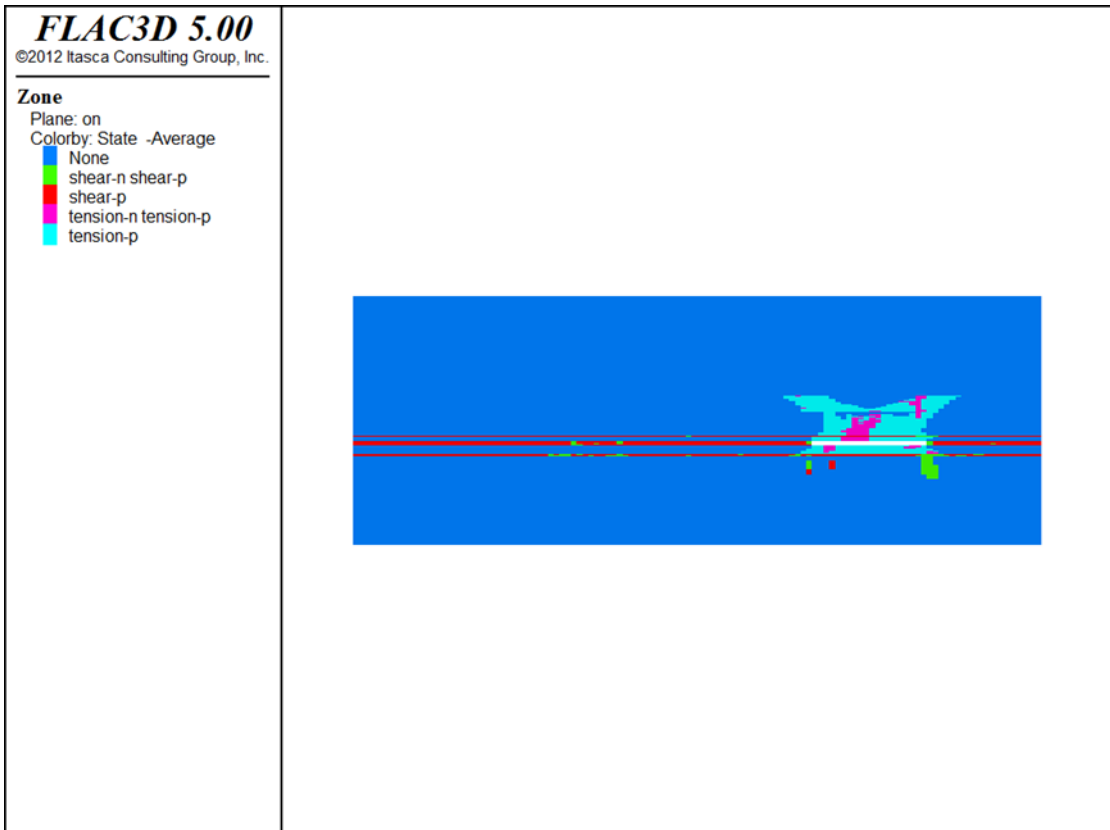
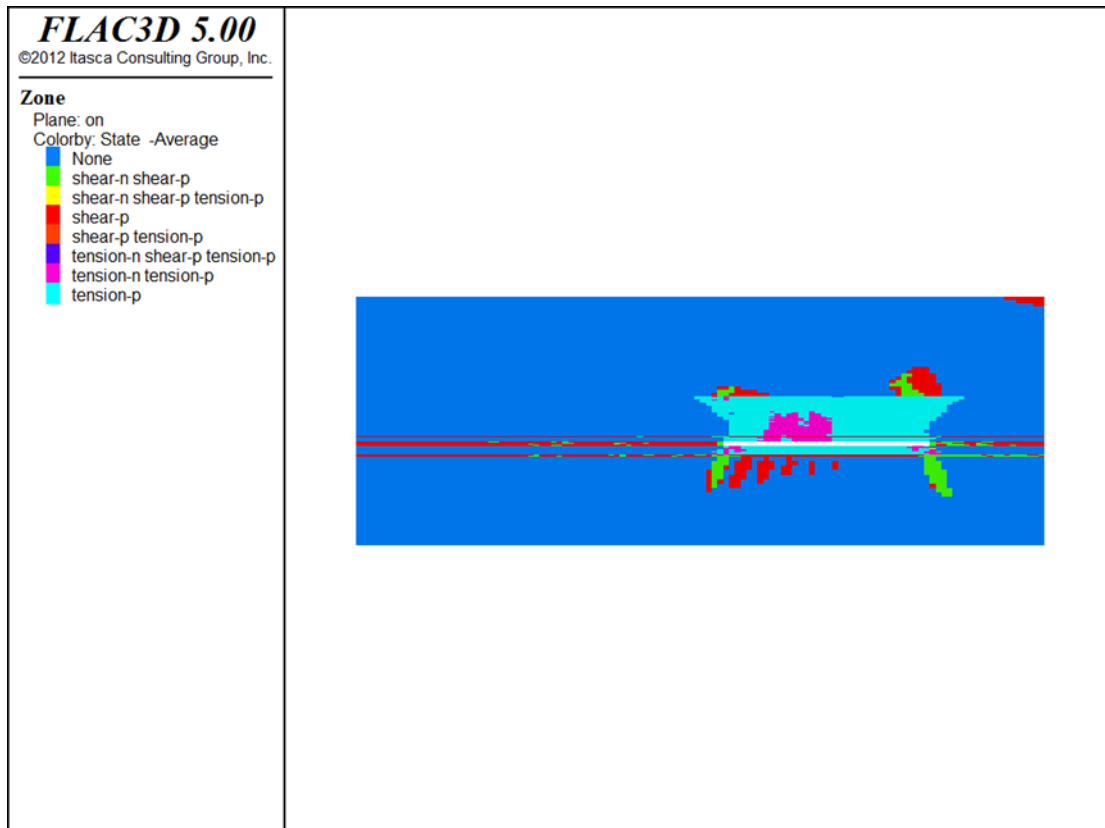


Figure 3.22. The damage state of the surrounding strata along strike direction after mining out 100m





**Figure 3.23. The damage state of the surrounding strata along strike direction after mining out 200 m**

The damage of plastic state of the model is acquired through observing the failure of the model in tension and shear, expressed in different color as can be seen in the figures (Figure 3.18-3.23). What is more, the model presents information if the stresses in the vicinity of mined-out area are on yield surface experiencing the in failure in shear and tension at the current step of excavation or stresses within the excavated area are fallen below the stress yield surface, indicating failure in previous excavation step. For instance, when the model was excavated to 100 meters (Figure 3.22), the zone around excavation experiences tension-n (failure in tension currently) and tension-p (failure in tension in previous run of the model).

With continuous advancement of working face, the overlying the stope strata experiences failure in tension.

As coal stratum begins to be mined, the failure initially occurred along the roof and floor of mined out coal seam and both shear and tension failure are occurring as can be observed in Figure 3.18 and Figure 3.21. These failures occurred as mining of working face advances are fractures.

After excavating 100 meters along strike (Figure 3.22), the change in plastic state of the model resembles the shape of "saddle" and the heights of plastic damage is lower in the middle compared to the failure experienced on each side of excavation area. The explanation to this phenomenon can be that on either side of the stope the barrier coal pillars are left and thus the conclusion that the compaction in the central area of the stope is higher than on two sides of the stope can be made. Also therefore indicating that the middle of the stope will experience more serious extent of collapse of overlying strata compared to either side of mined-out area.

However, with the advance of working face to 200 meters (Figure 3.20), the damage in the overlying strata forms in the shape resembling "O" shape, which is in accordance with findings from previous researchers.

The scope of tensile failure increases over larger area as larger volumes of coal are being extracted. Consequently, resulting in the gradual increase of distribution of the fractures as working face moves forward.

By observing the results of model element state, the conclusion of the height of fractured zone can be made. Before the simulation was conducted, the height of the fractured zone was found according to the Table (3.1) as for the medium strong rock to be 40.89 (m). The height of the fractured zone according to the results of simulation is 40 meters. Thus, the height of fractured zone obtained from the results of numerical simulation and empirical estimation are in accordance which therefore proves the validity of simulation.

With the increase of mined-out area the extent of deformation zone in the overlying strata will increase while the vertical stress in the zone will decrease.

---

### **3.6 Summary**

---

The conclusion of development of cracks through observing the results of the simulation can be made. Analyzing the results from vertical stress distribution, the potential region for the generation of cracks is in the zone of neutral stress between counteracting stresses from upper and lower sides. The fracture is expected to generate in the zone where stress values  $-5 \cdot 10^6$  MPa and  $1.0709 \cdot 10^6$  MPa as can be seen in the figure 3.11 when 200 m of coal is mined out. With the proceeding of the excavation of coal, the vertical displacement exhibits gradual increase in its value, thus proving that with the bigger excavation of coal mined, the height of the fractured zone will increase accordingly. The

conclusion of bigger the height of fractured zone the bigger the amount of fractures in the zone can be withdrawn.

What is more, the plastic zone displays deformation that model undergoes when the coal excavation takes place. Mainly the deformation of the model can be observed to be in the overlying rock strata above the stope. Moreover, the approximate height of fractured zone is estimated, which is in accordance with the empirical estimation of height of fractured zone proving the validity of the simulation.

---

## 4 Simulation of gas migration in goaf by FLUENT

---

In order to simulate the flow of methane from ventilation of working face into the goaf, the simulation model using FLUENT software was established. The simulation does not consider the change in temperature, regarding the air and methane as incompressible gasses.

---

### 4.1 Geometry of the model

---

The mesh of the model which is the input to FLUENT was generated using GAMBIT software to do so. First of all, the model was simplified in accordance with establishing intake and outflow airways, goaf and working face as can be seen in (Figure 4.1). Basic model dimensions are as follow: roadway width of 5 meters, the height of 4 meters and length of 10 meters, the dimensions of goaf with length of 200meters, height of 10 meters and 300 meters wide and working face with length of 200 meters, 4 meters high and 5 meters wide. The working face implements a “U” type of ventilation at approximately 224.50  $m^3/min$ .

To completely imitate the situation, the length of goaf is set to be 200 m for CFD base model.

The model is 300 m wide in X-direction, 200 m long in Y-direction and 10 m high in Z-direction as can be seen in figure 4.1. The model consists of 604400 cells, 1879400 faces and 671136 nodes.

The value of height of goaf is calculated empirically through estimating the height of caving zone using equation (3.1).

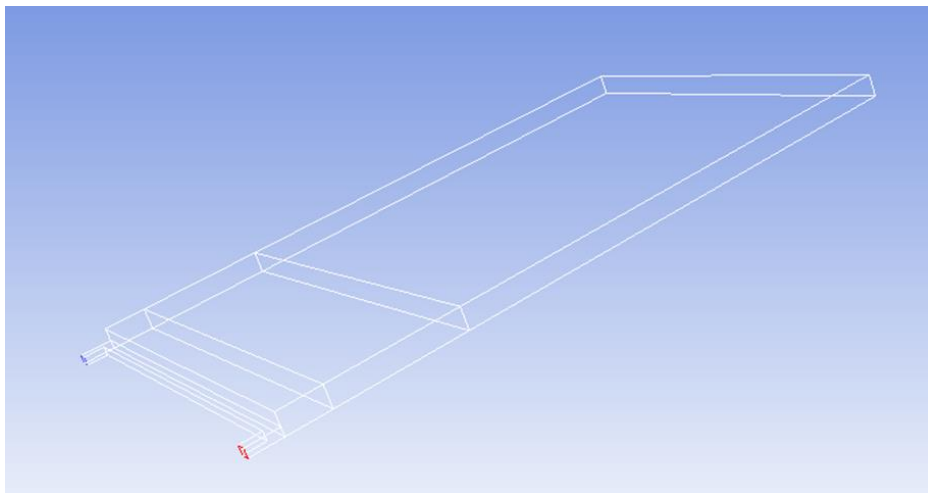


**Figure 4.1 Geometric model of goaf**

---

## 4.2 Boundary conditions

---

The gas in the model is regarded as mixture of air and methane. The gas flow follows governing equations of FLUENT software, which are equations of mass conservation, momentum equation and energy equation.

The flow of air in goaf is considered to be laminar due to low velocity.

In order to specify turbulence quantities when air flow enters the inlet, far-field boundary or outlet turbulence quantities such as turbulence intensity and hydraulic diameter to be set as boundary conditions.

Hydraulic diameter is generally regarded as “characteristic length” that is used for determination of dimensionless Reynolds number in order to determine whether the flow is turbulent or laminar. Hydraulic diameter in simulation model is set to be 4.4 m. Hydraulic diameter is calculated using the formula (4.7)

$$d = 4 \frac{A}{S} \quad (4.7)$$

where: A-cross section area,  $m^2$ ; S-perimeter, m

Moreover, another parameter used to set boundary condition is Turbulence intensity, I. Turbulent intensity is calculated by formula (4.8).

$$I = 0.16 \left( \frac{v d \rho}{\mu} \right)^{-\frac{1}{8}} \quad (4.8)$$

Where:  $\rho$ -density,  $kg/m^3$ ;  $\mu$ -kinematic viscosity, Pa·s;  $v$ -velocity at inlet, m/s;  $d$ -hydraulic diameter, m. The Turbulence intensity is equal 2.5 %.

The intake airflow roadway is set to velocity inlet while return airway is set to outflow. The velocity magnitude in inlet is calculated by dividing volume of air supplied into the working face to area. So, the velocity is calculated:

$$V = 1224.50 \frac{m^3}{min} \div 20 m^2 = 1.02 \frac{m}{s} \quad (4.9)$$

In order to simulate turbulent flow situation, relevant turbulent model to be set up. For this model, k epsilon turbulence model was established.

Having taken into consideration the division of three zones in longitudinal direction, the area of the goaf was divided into 3 zones according to porosity. Zone 1 is the zone, which is closest to the working face has highest porosity equal to 0.24. Second zone of goaf, further

away from the working face, has the porosity of 0.18. Third zone the most distant from working face has the lowest porosity equal to 0.1.

The amount of air exhaust gas is  $15.5 \text{ m}^3/\text{min}$  and 70 % of it is gas emission in the goaf.

So, the gas source term in goaf is:

$$15.5 \times 70 = 10.85 \text{ m}^3/\text{min}$$

With gas density  $0.7 \text{ kg/m}^3$ , the source of gas in goaf is:

$$\frac{10.85 \times 0.7}{60 \times 200 \times 10 \times 300} = 2.11e^{-7} \left( \frac{\text{kg}}{\text{m}^3} \cdot \text{s} \right) \quad (4.10)$$

Based on the length of each part average bulging coefficient is:

$$\frac{1.4 \times 20 + 1.3 \times 60 + 1.1 \times 220}{300} = 1.16 \quad (4.11)$$

Where 1.4, 1.3 and 1.1 are the bulging coefficients of each zone

Gas term for each zone is determined as follow:

Gas term of zone 1:

$$\frac{1.4 \times 20}{1.16 \times 300} \times 2.11e^{-7} = 1.69e^{-8} (\text{kg/m}^3 \cdot \text{s}) \quad (4.12)$$

Gas term of zone 2:

$$\frac{1.3 \times 60}{1.16 \times 300} \times 2.11e^{-7} = 4.7e^{-8} (\text{kg/m}^3 \cdot \text{s}) \quad (4.13)$$

Gas term of zone 3:

$$\frac{1.1 \times 220}{1.16 \times 300} \times 2.11e^{-7} = 1.43e^{-7} (\text{kg/m}^3 \cdot \text{s}) \quad (4.14)$$

---

### 4.3 Gas seepage characteristics

---

Since the goaf area is considered to be porous medium, the source term of fluid momentum loss is described in the following equation (4.1) (Zhang et al., 2011). In this equation

the source term consists of two parts: the inertial loss term second part of the right side of the equation (4.1) and the viscous loss term the first part of the right side of the equation (4.1).

$$S_i = -\left(\sum_{i=1}^3 D_{ij} \mu \vartheta_j + \sum_{i=1}^3 C_{ij} \frac{1}{2} \rho |\vartheta| \vartheta_j\right) \quad (4.1)$$

Where:  $S_i$  source term for  $i$ th (x,y or z) equation;  $\mu$ -the viscosity; D and C-prescribed matrices;  $|\vartheta|$ -vector of the velocity magnitude;  $\vartheta$ -the velocity component of the source in x, y, z direction.

Typically, with laminar flow of the fluid through porous medium pressure drop is proportional to the velocity. The porous media model can then be reduced to the Darcy's Law in porous media, ignoring the liquid inertial loss (Zhang et al., 2011).

$$S_i = -\frac{\mu}{\alpha} \vartheta \quad (4.2)$$

Where:  $\alpha$ -the permeability,  $m^2$

---

#### 4.4 Gas governing equations

---

The Navier-Stokes equation in porous medium can be used under assumption that gas flow in goaf is incompressible flow (Zhang et al., 2011)

$$\frac{\partial(\rho Y_s)}{\partial t} + \frac{\partial}{\partial x_j} (\rho Y_s u_j) = \partial \left( \rho D_s \frac{\partial Y_s}{\partial x_j} \right), (s = 1, 2, \dots, n_s) \quad (4.3)$$

$$\frac{\partial(\rho u_i)}{\partial t} + \frac{\partial}{\partial x_j} (\rho u_i u_j + \delta_{ij} p) = \frac{\partial \tau_{ij}}{\partial x_j} + S_i \quad (4.4)$$

$$\frac{\partial(\rho E)}{\partial t} + \frac{\partial}{\partial x_j} (\rho H u_j) = \frac{\partial}{\partial x_j} \left( \tau_{ij} u_j + \frac{\partial T}{\partial x_j} \right) \quad (4.5)$$

$$p = \rho T R_u \sum_{s=1}^{n_s} \frac{Y_s}{M_s} \quad (4.6)$$

$\rho$ -density of mixture, g/m; T-time variable;  $u_i$  and  $u_j$ -velocity, m/s;  $\delta_{ij}$ -"Knocker delta"

P-pressure, Pa;  $\tau_{ij}$ -shear stress tensor of molecular;  $S_i$ -the source item of momentum loss; E-the energy in per volume, J; H-the total enthalpy in per volume, J/mol; k-the heat transfer coefficient of fluid; T-the static temperature, K;  $n_s$  the sum of components;  $R_u$  universal

constant;  $M_s$  Molecular weight;  $Y_s$  -mass concentration;  $D_s$  mass diffusion coefficient;  $h_s$  -the value of absolute enthalpy of unit mass

In the above mention governing equations, equation 4.3 is the continuum equation, equation 4.4 is the momentum equation and 4.5 is the energy equation, and equation 4.6 is the equation for ideal gas of mixtures.

---

## **4.5 Results of the simulation**

---

Velocity distribution, pressure distribution as well as mass fraction of methane are the results of the simulation. Through identifying the low velocity zone and then identifying the region in goaf where the mass fraction of methane is high, the identification of the potential gas accident region will be distinguished.

---

### **4.5.1 Velocity distribution**

---

The velocity of air entering the ventilation system is approximately in range of 1.18(m/s), air hitting the goaf slows down to about 0.42(m/s). According to the results of simulation, the highest recorded velocity is 1.690025 (m/s). What is more, from further analyzing wind velocity distribution, it is evident that the lowest velocity can be observed in the upper corner of the goaf. This phenomenon can be explained through formation of vortex of air in that corner of the goaf. Thus, the potential of gas accidents in the upper corner of the goaf is higher in this region. The velocity entering the ventilation system in inlet is set to 1.02 (m/s).





Figure 4.2. Distribution of velocity

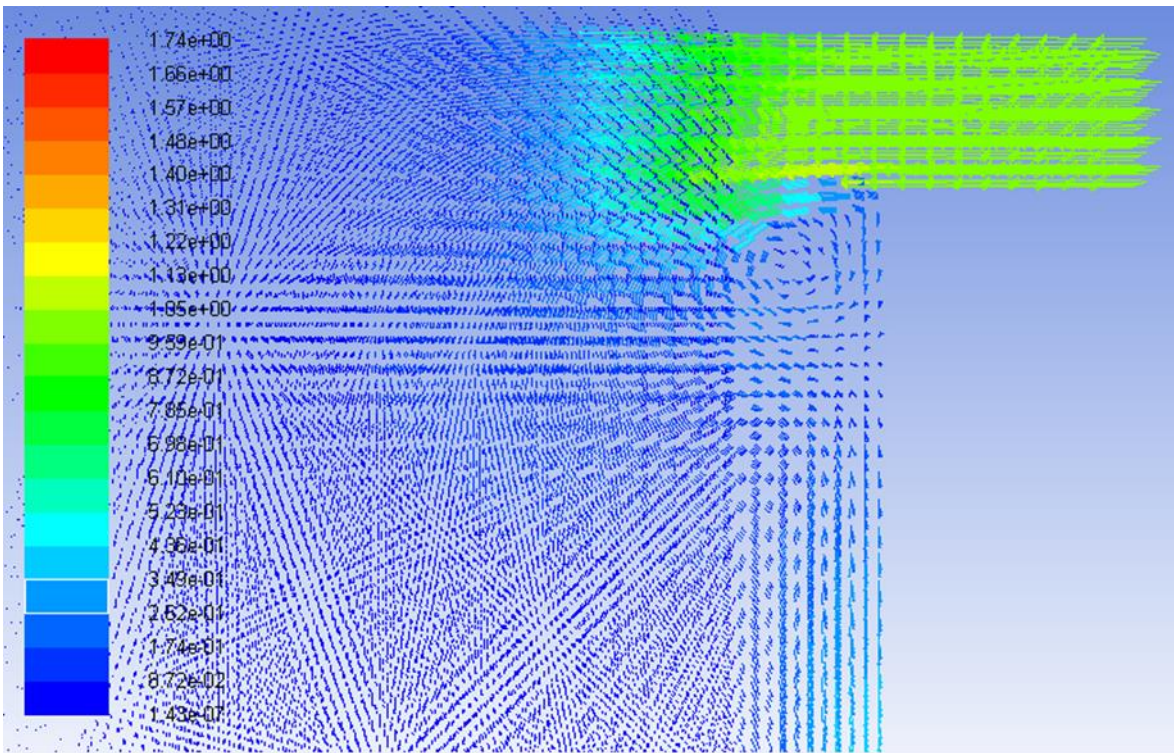
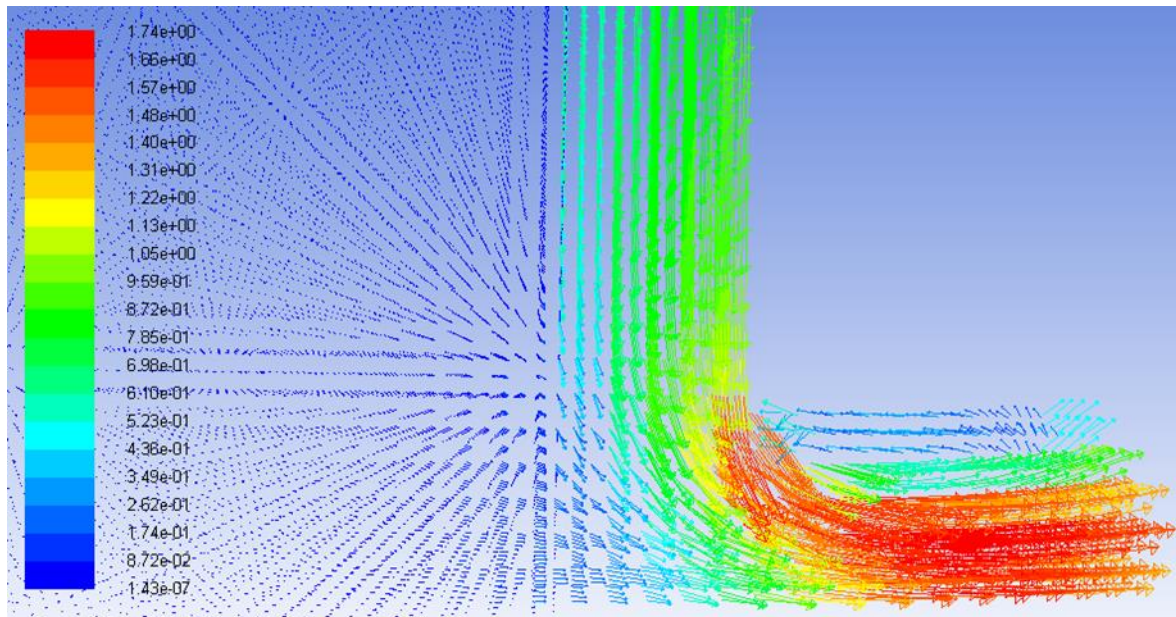


Figure 4.3. The distribution of velocity presented in vectors in the inlet



**Figure 4.4 The distribution of velocity presented in vectors in the upper corner of goaf**

#### **4.5.2 The mass fraction of methane distribution**

Whilst methane liberates from coal seams due to mining, it flows and tends enter gob area through air leakage. The results of the simulation model display that methane has tendency of uneven distribution pattern in goaf. It can be seen from figure 4.5 that the methane concentration increases from the area close to working face to depth of caving region and from intake to return airway. The range of mass fraction of methane in goaf varies from zero to one. The lowest magnitude of methane concentration can be observed in the first zone. According to analysis of data from simulation, zone number three is region with highest anticipated mass fraction of methane. This can be explained due to different porosities of goaf in corresponding areas. “U” type of ventilation implemented at the working face can result in driving the methane into deeper parts of caving region and due to the movement of air within the goaf upwards the methane will accumulate in high concentration in the upper corner of goaf. Thus, forming the region of high methane concentration in the upper corner of goaf area.

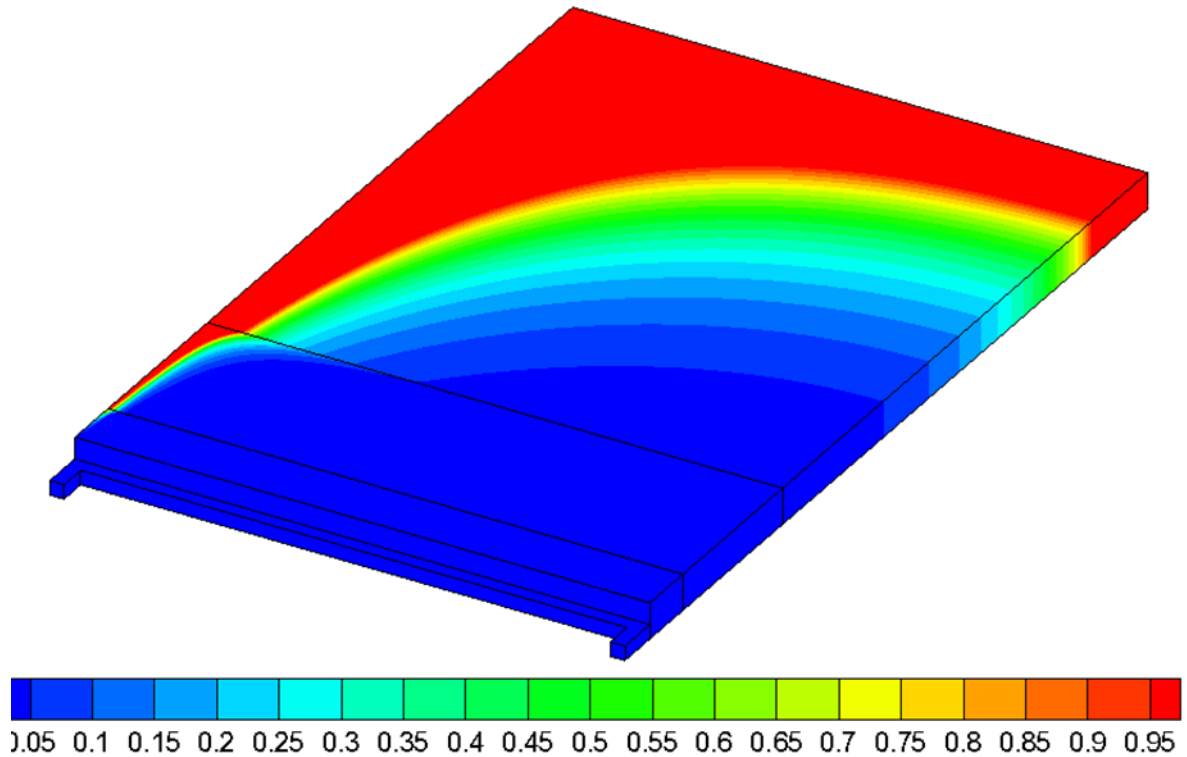


Figure 4.5 The distribution of mass fraction of methane

#### 4.5.3 Pressure distribution

Analyzing the results of simulation model, there has been registered pressure difference in inlet and outlet. The greater pressure can be observed in the inlet. Maximal pressure is registered in the entrance of air in inlet at the first zone of goaf with corresponding value of 0.790479 (Pa). While the lowest pressure can be observed in the outlet with value of -2.336779 (Pa) accordingly. This can be explained through basic principle of ventilation that air will move from positive pressure (high) to negative pressure (low) thus creating pressure difference is essential.

From observing the results of simulation, pressure distribution in vertical direction it is evident that the pressure in the upper part of the goaf is higher than in lower part due to higher concentration level of methane in the upper part of the goaf.



**Figure 4.6. Distribution of pressure**

---

## 4.6 Summary

---

The distribution of methane, velocity of air and contour of distribution of pressure are the obtained results from the simulation. The highest pressure is observed in the inlet contrary lowest value of pressure can be observed in the outlet. High concentration of methane is observed to be in the upper corner of goaf. This can be explained that due to implementation of “U” type of ventilation, air flowing into the goaf will contribute to methane flowing towards upper corner following air leakage. Since the simulation results presented the lowest velocity in the upper corner of goaf due to formation of air vortex in the zone, this region is considered to be potential zone where gas accidents will take place. Therefore, the upper corner of goaf is subject of investigation for methane drainage and Chapter 5 will focus on measure to reduce methane accumulation in this area.

---

## **5 The design of the methane drainage**

---

In order to drain gas from goaf area and overlying the goaf area, this research proposes implementing high-level and low-level drill-holes as well as placement of pipe in the upper corner of goaf area.

---

### **5.1 Formation of annular fissure circle**

---

When mining reaches some point, the fractures in the roof rock in the middle of goaf area tend to be compacted, there are connected crack development region around goaf, which is similar in shape of “O” ring. The explanation of "O"-ring formation of fractures in the roof strata above stope can be given by analyzing caving of the roof strata, strata above the stope will tend to fall down and cave, but it will not fully collapse due to existence of coal pillars forming hollow cracks in the roof. These fractures will not be experiencing compaction for considerably long period of time with boundary of fracture zone resembling annular ring (Liu et al., 2004).

It has been found out that after coal extraction dynamically changing fracture zones will take place in the overlying strata. With the advancement of working face, the vertical three zones, horizontal three zones and transverse three zones also move forward, intersecting with one another at some point resulting in fissures in the fractured zone and rocks of caving zone area experiencing once again compaction owing it to mitigation of overburden rock mass. This place of intersection forms a region with high regional gas concentration around goaf known as annular fissure circle (Li, 2000; Liu and Yuan, 2004) in (Zhang et al. 2012).

The permeability value not only increases twice the original value, but also the area of formation of "O" circle is considered to be larger than compaction zone. Thus, the formation of "O" circle enhances the propagation fractures and permeability in the area providing sufficient flow pathways enough for gas to desorb, dissipate, permeate and accumulate in overburden strata above goaf area (Zhang et al 2012).

Since the "O" ring formation has been recognized, more attention has been paid to pressure-relief gas drainage in goaf area (Liu et al., 2004).

---

## **5.2 The principle of high level drill hole**

---

As mining advances, along with the progress of advancing of the working face, a pressure field is formed around working face. Along with pressure field, stress field is formed due to its influence “three zones” are formed in the vertical and longitudinal directions the fractures created in this pressure field become channels for gas flow and migration (Li et al., 2013).

The principle of using high-level drill holes for drainage of gas in the upper corner is based on the assumption of rock movement and origination of annular “O” fissure zone of crack distribution of goaf and the location of end of borehole is set to be within the development of cracks in the roof (Li, 2018).

With the advancement of working face, the goaf will be formed behind working face due to implementation of “U” type of ventilation. The gas accumulated in the goaf area through the fractures in the roof will float to the “O” ring of mining fractures, since the density of methane is smaller than that of air. If the final hole position of drill hole is arranged in fractured zone, the drill hole will be in the upper part of “O” ring. Negative pressure zone formed due to drilling terminal, changes the direction of the movement of gas in the goaf. Negative pressure can be used to accelerate gas flow through implementation of borehole drainage. So that high-level borehole can effectively extract the gas, and the amount of gas extracted can greatly surpass gas content of coal seam (Li et al., 2013).

Due to having differences in lithology of coal seams, the roof and overlying strata in different mining areas, have different heights of caving, fractured and bent deformation zones. In order to achieve better drainage result, prior to designing high-level drilling parameters, it is suggested by most fundamental approach of achieving best drainage result is to determine firstly the range of heights of caving and fractured zones through investigation of the law of roof strata caving and examining the distribution of cracks in the goaf (Nie, 2008: Li, 2018).

---

## **5.3 Selection of drilling location**

---

The annular fissure zone is the primary region for drainage of gas in the adjoining coal seam and it is the chief placement area for the arrangement of drill holes in adjoining seam. Particularly, the fissure circle that is formed at the upper corner of intersection

between tailgate and working face is the core region for gas drainage in adjoining seam (Zhang et al., 2012).

The essential part of effective high-level drilling is to select the best position of drill hole and ensure horizontal distance of drill hole from return airway as well as ensuring the drill hole placement in the fractured zone above the upper part of fractured zone. To do so, the law of roof strata falling and distribution of fractures in the goaf has to be analyzed (Nie, 2008).

It was found out based on the law of movement of overlying strata and the law of gas flow that the fractured zone is most developed in the middle and lower parts. Being the key accumulation area of gas, the area of lower and middle section of fractured zone is the region with high gas content and high concentration. This area not only is best location of borehole placement, but also is also best area for drilling high-level drill holes (Li, 2013).

The best position for gas drainage when tail roadway is selected as position for gas drainage drill holes is in the vicinity of very beginning of generation of separation zone and fracture zone before subsidence and compaction are fully carried out. The better drainage results are accomplished by positioning the drainage drill hole a certain distance in front or behind the working face (Zhang et al., 2012).

---

#### **5.4 High level drill hole parameters design**

---

As a result of existing pressure difference between fracture-formed channels and roadways, gas will tend to liberate and to dissipate to the area of working face by doing so emission of gas in the upper corner of fissure circle of working face will increase and gas concentration in that area is expected to surpass the limit (Zhang et al., 2012).

Based on law of gas flow as well as movement of overlying strata, the zones of middle and lower part of fracture zone to be sufficiently developed, and act as main areas of gas accumulation. These areas have high gas content and high gas concentration, acting not only as best gas extraction areas, but also best position for drilling of holes (Li 2004).

According to (Zhang et al., 2012) recommendations the place where annular fissure circle locates as well as principle of gas seepage, for drill hole design and arrangement so as to put off the possibility of damaging drill hole and ensure better drainage results. Following principles should be followed:

Drill hole position should not be oriented too high into separation zone, and shall be position wither on the central of lower part of the fissure zone.

High dip drill hole shall be placed not too low so as to prevent its damage indicating that the high dip drill hole should be placed above caving zone at the distance of 1.5 times the mining height.

Drill hole should go into intersection between separation and compaction zones or in the middle of separation zone in longitudinal direction to ensure efficient gas drainage results.

---

## 5.5 The design of drill holes

---

The final hole position should be located in the development range of roof cracks between caving and fractured zones. Therefore, the height of the high-level drilling borehole should meet the following condition:

$$H_m < H_z < H \quad (5.1)$$

Where:  $H_m$ - the height of caving zone, m;

$H$ -the height of fractured zone, m

$H_z$ -the height of the high-level drilling height, m

Due to accumulation of high concentration of gas in the annular fissure circle, the boreholes are designated to be placed within this zone. The results of the simulation (Figure 3.18) displayed the location of annular fissure circle above goaf area. The results of the simulation by FLAC3D indicated the height of the fractured zone to be 40 meters. Therefore, the highest borehole location should be positioned at 39.5 m referring. What is more, the results of the simulation of cracks propagation in the overlying strata displayed the uniform distribution of fractured zone in the overlying strata above ventilation roadway (Figure 3.18). This will consequently mean the final drill hole position will have uniform distribution.

As mentioned in previous Chapter 3, the height of caved zone was acquired empirically and it is estimated to be 8.86 meters. Therefore, according to the formula (5.1) the height of borehole placement from coal seam roof is selected to be within the range  $8.86\text{m} < H_z < 40\text{m}$ . To ensure the stability of borehole, the minimum height of drill hole in this research was selected to be higher than estimated caving zone. As well as maximal height of the drill hole is set to be 39.5 meters, which is less than the height of the simulated



result of the approximate height of the fractured zone. In order to ensure the stability of borehole and prevent the rock from falling and collapsing blocking the borehole, the final hole position is designed to be between layers of siltstone and mudstone, which is considered to be relatively stable rock formations.

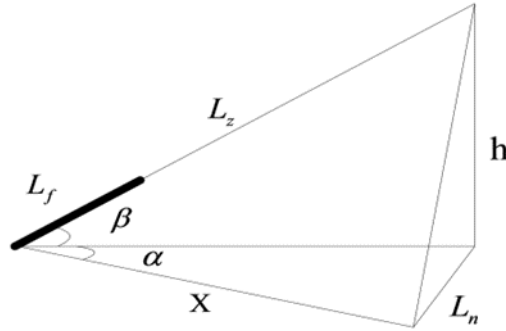


**Figure 5.1 The relationship between the parameters of the drill hole**

In the figure 5.1 the borehole is directed from ventilation roadway towards the overlying strata of the ventilation roadway, it is inclined at an angle  $\beta$ .

The vertical height of the drill hole:

$$h = \frac{X \cdot \tan \beta}{\cos \alpha} = L_z \sin \beta \quad (5.2)$$

The horizontal projection of length of borehole:

$$L_g = L_z * \cos \beta \quad (5.3)$$

The horizontal distance from projection of end of drill hole to the roadway:

$$L_n = L_z \times \cos \beta \times \cos \alpha \quad (5.4)$$

Projection length of borehole on roadway direction:

$$X = L_z \times \cos \alpha \times \cos \beta \quad (5.5)$$

In equations (5.2-5.5)  $L_z$  is the total length of the borehole;  $\beta$  is the dip angle of the borehole;  $L_f$  is the sealed length of borehole;  $\alpha$  is the angle between horizontal projection of borehole and roadway.

The boreholes were put together into groups and divided into 7 drilling sites. Each borehole within drill site was designated with two numbers for identification purposes. First digital representing the number of drill site and latter referring to the number of borehole

within the drilling field. For instance, second drill hole of the first drill site was marked as 1-2. With the aim of maximizing efficiency of methane drainage, drill holes with matching second number of identification were designed to have the same parameters of inclination angle, azimuth and depth of borehole. Thus, the boreholes were targeted in the same location leaving no blank space left to increase the drainage efficiency. To accommodate maximal capture efficiency of methane drainage, the implementation of boreholes with overlapping areas of 20 meters was chosen in design.

Taking into consideration the length along strike 1434.7, the total number of seven drilling fields were designed. Taking into account the experience of borehole drilling in China generally from 10 to 15 drill holes comprise one group, the total number of boreholes in each drill site is selected to be 12 drill holes. Out of 12 drill holes, seven were selected to be high-level drill holes and the remaining five as low-level boreholes. Considering that high-level boreholes will drain the methane in overlying strata and low-level boreholes will aim at the upper corner of goaf where methane accumulates due to air leakage. The boreholes are arranged implementing fan-shaped drilling configuration. The spacing between two adjacent drilling fields was chosen to be 80 meters. Based on the consideration that distance between drill sites is 80 meters, the range of borehole the length of borehole were varied ranging from 99-109 meters. The distance between drill hole opening the ventilation roadway was chosen to be 2 m.

Since the parameters of boreholes are the same, the calculation of one drilling site can be applied to other drilling sites as well. The calculation of drilling parameters for first drilling site is given below.

---

### 5.5.1 Calculation of drilling parameters for high-level drill hole

---

Based on the equations (5.2-5.5) of parameters of high-level and low-level drill holes were derived.

1-1

H=39.5 m;  $\alpha$ -38°;  $L_z$ -109m

$$H = L_z * \sin\beta \quad (5.6)$$

$$\sin\beta = \frac{H}{L_z} \quad (5.7)$$

$$\beta = \arcsin \frac{H}{L_z} \quad (5.8)$$

$$\beta = \arcsin \frac{39.5}{109} = 21.2476(^{\circ}) \quad (5.9)$$

$$L_g = L_z * \cos \beta \quad (5.10)$$

$$L_g = 109 * \cos(21.2476) = 101.5905(m) \quad (5.11)$$

$$L_n = L_z * \sin \alpha * \cos \beta \quad (5.12)$$

$$L_n = 109 * \sin(38) * \cos(21.2476) = 62.5474(m) \quad (5.13)$$

$$X = L_z * \cos \alpha * \cos \beta \quad (5.14)$$

$$X = 109 * \cos(38) * \cos(21.2476) = 80.0544 (m) \quad (5.15)$$

1-2

H=37 m;  $\alpha = -34^{\circ}$

$$\beta = \arcsin \frac{37}{108} = 20.0353(^{\circ}) \quad (5.16)$$

$$L_g = L_z * \cos \beta \quad (5.17)$$

$$L_g = 108 * \cos(20.0353) = 101.464(m) \quad (5.18)$$

$$L_n = L_z * \sin \alpha * \cos \beta \quad (5.19)$$

$$L_n = 108 * \sin(34) * \cos(20.0353) = 56.7379(m) \quad (5.20)$$

$$X = L_z * \cos \alpha * \cos \beta \quad (5.21)$$

$$X = 108 * \cos(34) * \cos(20.0293) = 84.1175(m) \quad (5.22)$$

1-3

H=34;  $\alpha = -32^{\circ}$

$$\beta = \arcsin \frac{34}{107} = 18.5238(^{\circ}) \quad (5.23)$$

$$L_g = 107 * \cos(18.1738) = 101.4565(m) \quad (5.24)$$

$$L_n = 107 * \sin(32) * \cos(18.1738) = 53.7637(m) \quad (5.25)$$

$$X = 107 * \cos(32) * \cos(18.1738) = 86.04(m) \quad (5.26)$$

1-4

H=28;  $\alpha - 28^\circ$

$$\beta = \arcsin \frac{28}{106} = 15.3135(^\circ) \quad (5.27)$$

$$L_g = 106 * \cos(15.3135) = 102.2365(m) \quad (5.28)$$

$$L_n = 106 * \sin(28) * \cos(15.3135) = 47.9971(m) \quad (5.29)$$

$$X = 106 * \cos(28) * \cos(15.3135) = 90.2695 (m) \quad (5.30)$$

1-5

H=25;  $\alpha - 26^\circ$

$$\beta = \arcsin \frac{25}{105} = 13.9101(^\circ) \quad (5.31)$$

$$L_g = 105 * \cos(13.9101) = 101.9207(m) \quad (5.32)$$

$$L_n = 105 * \sin(26) * \cos(13.9101) = 44.6791(m) \quad (5.33)$$

$$X = 105 * \cos(26) * \cos(13.9101) = 91.6057 (m) \quad (5.34)$$

1-6

H=22; $\alpha - 24^\circ$

$$\beta = \arcsin \frac{22}{104} = 12.2103 (^\circ) \quad (5.35)$$

$$L_g = 104 * \cos(12.2103) = 101.6473(m) \quad (5.36)$$

$$L_n = 104 * \sin(24) * \cos(12.2103) = 41.3437(m) \quad (5.37)$$

$$X = 104 * \cos(24) * \cos(12.2103) = 92.8594 (m) \quad (5.38)$$

1-7

H=19;  $\alpha - 20^\circ$

$$\beta = \arcsin \frac{19}{103} = 10.6319 (^\circ) \quad (5.39)$$

$$L_g = 103 * \cos(10.6319) = 101.2317(m) \quad (5.40)$$

$$L_n = 103 * \sin(20) * \cos(10.6319) = 34.6233(m) \quad (5.41)$$

$$X = 103 * \cos(20) * \cos(10.6319) = 95.1267 (m) \quad (5.42)$$

1-8

H=16;  $\alpha = 16^\circ$

$$\beta = \arcsin \frac{16}{102} = 9.0212 (^\circ) \quad (5.43)$$

$$L_g = 102 * \cos(9.0212) = 100.7383(m) \quad (5.44)$$

$$L_n = 102 * \sin(16) * \cos(9.0212) = 27.7672(m) \quad (5.45)$$

$$X = 102 * \cos(16) * \cos(9.0212) = 96.8358 (m) \quad (5.46)$$

1-9

H=13;

$$\beta = \arcsin \frac{13}{101} = 7.3945 (^\circ) \quad (5.47)$$

$$L_g = 101 * \cos(7.3945) = 100.16(m) \quad (5.48)$$

$$L_n = 101 * \sin(12) * \cos(7.3945) = 20.8244(m) \quad (5.49)$$

$$X = 101 * \cos(12) * \cos(7.3945) = 97.9713 (m) \quad (5.50)$$

1-10

H=10;  $\alpha = 8^\circ$

$$\beta = \arcsin \frac{10}{100} = 5.7392 (^\circ) \quad (5.51)$$

$$L_g = 100 * \cos(5.7392) = 99.4987(m) \quad (5.52)$$

$$L_n = 100 * \sin(8) * \cos(5.7392) = 13.8475(m) \quad (5.53)$$

$$X = 100 * \cos(8) * \cos(5.7392) = 98.5304 (m) \quad (5.54)$$

1-11

H=9.5;  $\alpha = 6^\circ$

$$\beta = \arcsin \frac{9.5}{99.5} = 5.4743 (^\circ) \quad (5.55)$$

$$L_g = 99.5 * \cos(5.2154) = 99.0462(m) \quad (5.56)$$

$$L_n = 99.5 * \sin(6) * \cos(5.4743) = 10.3531(m) \quad (5.57)$$

$$X = 99.5 * \cos(6) * \cos(5.4743) = 98.5036 (m) \quad (5.58)$$

1-12

H=9.3;  $\alpha = 4$

$$\beta = \arcsin \frac{9.3}{99} = 5.3880(^{\circ}) \quad (5.59)$$

$$L_g = 99 * \cos(5.3880) = 98.5626 (m) \quad (5.60)$$

$$L_n = 99 * \sin(4) * \cos(5.3880) = 6.8754(m) \quad (5.61)$$

$$X = 99 * \cos(4) * \cos(5.3880) = 98.3225 (m) \quad (5.62)$$

Drill site	Drill hole number	Azimuth (°)	Dip (°)	Drill hole length (m)
1	1-1	38	21.2476	109
	1-2	34	20.0353	108
	1-3	32	18.5238	107
	1-4	28	15.3135	106
	1-5	26	13.9101	105
	1-6	24	12.2103	104
	1-7	20	10.6319	103
	1-8	16	9.0212	102
	1-9	12	7.3945	101
	1-10	8	5.7392	100
	1-11	6	5.4743	99.5
	1-12	4	5.3880	99
2	2-1	38	21.2476	109
	2-2	34	20.0353	108
	2-3	32	18.5238	107
	2-4	28	15.3135	106
	2-5	26	13.9101	105
	2-6	24	12.2103	104
	2-7	20	10.6319	103
	2-8	16	9.0212	102
	2-9	12	7.3945	101
	2-10	8	5.7392	100

	2-11	6	5.4743	99.5
	2-12	4	5.3880	99
3	3-1	38	21.2476	109
	3-2	34	20.0353	108
	3-3	32	18.5238	107
	3-4	28	15.3135	106
	3-5	26	13.9101	105
	3-6	24	12.2103	104
	3-7	20	10.6319	103
	3-8	16	9.0212	102
	3-9	12	7.3945	101
	3-10	8	5.7392	100
	3-11	6	5.4743	99.5
	3-12	4	5.3880	99
4	4-1	38	21.2476	109
	4-2	34	20.0353	108
	4-3	32	18.5238	107
	4-4	28	15.3135	106
	4-5	26	13.9101	105
	4-6	24	12.2103	104
	4-7	20	10.6319	103
	4-8	16	9.0212	102
	4-9	12	7.3945	101



	4-10	8	5.7392	100
	4-11	6	5.4743	99.5
	4-12	4	5.3880	99
5	5-1	38	21.2476	109
	5-2	34	20.0353	108
	5-3	32	18.5238	107
	5-4	28	15.3135	106
	5-5	26	13.9101	105
	5-6	24	12.2103	104
	5-7	20	10.6319	103
	5-8	16	9.0212	102
	5-9	12	7.3945	101
	5-10	8	5.7392	100
	5-11	6	5.4743	99.5
	5-12	4	5.3880	99
6	6-1	38	21.2476	109
	6-2	34	20.0353	108
	6-3	32	18.5238	107
	6-4	28	15.3135	106
	6-5	26	13.9101	105
	6-6	24	12.2103	104
	6-7	20	10.6319	103
	6-8	16	9.0212	102

7	6-9	12	7.3945	101
	6-10	8	5.7392	100
	6-11	6	5.4743	99.5
	6-12	4	5.3880	99
	7-1	38	21.2476	109
	7-2	34	20.0353	108
	7-3	32	18.5238	107
	7-4	28	15.3135	106
	7-5	26	13.9101	105
	7-6	24	12.2103	104
	7-7	20	10.6319	103
	7-8	16	9.0212	102
7-9	12	7.3945	101	
7-10	8	5.7392	100	
7-11	6	5.4743	99.5	
7-12	4	5.3880	99	

**Table 5.1. Designed drilling parameters**

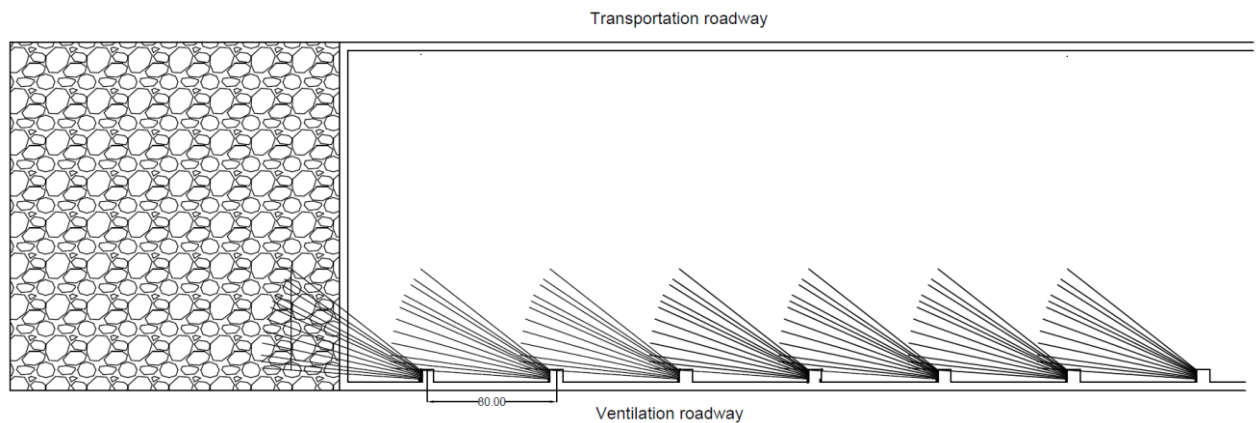


**Figure 5.2. The design of high-level and low-level drill holes in the overlying strata of goaf**

The outcome of the methane drainage design displays evenly distributed positioning of final boreholes, which will contribute to better drainage results.

---

## 5.6 Design of pipe in the upper corner

---

According to the technical document obtained from Qianjiaying mine, 7th coal seam is regarded as spontaneous combustible mine with the anticipated absolute gas emission of  $15.5 \text{ m}^3/\text{min}$  and the estimated volume of air to the working face is  $25 \text{ m}^3/\text{s}$ . The anticipated gas concentration before pumping is expected to be within the range 1%. After installation of pump the gas concentration will be 0.8% to ensure safe working conditions.

---

### 5.6.1 Calculation of design parameters

---

Diameter of pipe

In order to design the diameter of pipe the amount of gas pumped as well as absolute gas emission to the working face should be taken into consideration.

Flow rate of drainage pipe,  $Q_f$ :

The required amount of gas that needs to be pumped is considered through consideration of the amount of gas liberated to the working face as well as the amount of gas discharged by ventilation. The amount of gas pumped should follow the equation (5.63) thus it must be greater or equal to the difference between the amount of gas emitted to the working face and the amount of gas discharged by ventilation.

The amount of gas discharged by ventilation:

$$Q_f = \frac{25 \text{ m}^3}{\text{s}} \times 60 \times 0.8 = 12 \text{ m}^3/\text{min} \quad (5.63)$$

As mentioned previously, the absolute gas emission is  $15.5 \text{ m}^3/\text{min}$

Drainage pipe and high-level drill hole flow rate:

$$15.5 - 12 = 3.5 \text{ m}^3/\text{min}$$

The quantity of mixing gas or air:

$$Q = \frac{Q_c}{c} \quad (5.64)$$

$Q_c$  is gas flow in tube,  $\text{m}^3/\text{min}$ ;

$C$  is gas concentration in the gas pipe, %

Pre-drainage calculation by pumping  $3.5 \text{ m}^3$  gas

$$Q = 3.5 \text{ m}^3/\text{min} \div 15\% = 23.3 \text{ m}^3/\text{min}$$

Drainage concentration was selected to be 15%

Determination of pipe diameter:

$$D = 0.1457 \left( \frac{Q_h}{V} \right)^{\frac{1}{2}} \times 1000 \quad (5.65)$$

Where:  $v$  is the average flow velocity in pipe, m/s;

$D$  is the inner diameter of gas pipe, mm

Average flow rate of gas in pipeline is taken as 12 m/s

$$D = 0.1457 \times \left( \frac{23.3}{12} \right)^{\frac{1}{2}} \times 1000 = 203 \text{ (mm)} \quad (5.66)$$

In order to meet drainage requirements, drainage pipe diameter of 400 mm is selected.

Based on simulation results from FLUENT, high concentration of gas was detected in the upper corner part of the goaf area. Pipe with diameter of 0.4m and height of 30 m was selected for drainage. In practice, the buried depth of pipe is taken from 8 to 10 meters. Therefore, pre-embedded pipe was selected with the buried depth of the 8 meters as shown in the Figure 5.3.

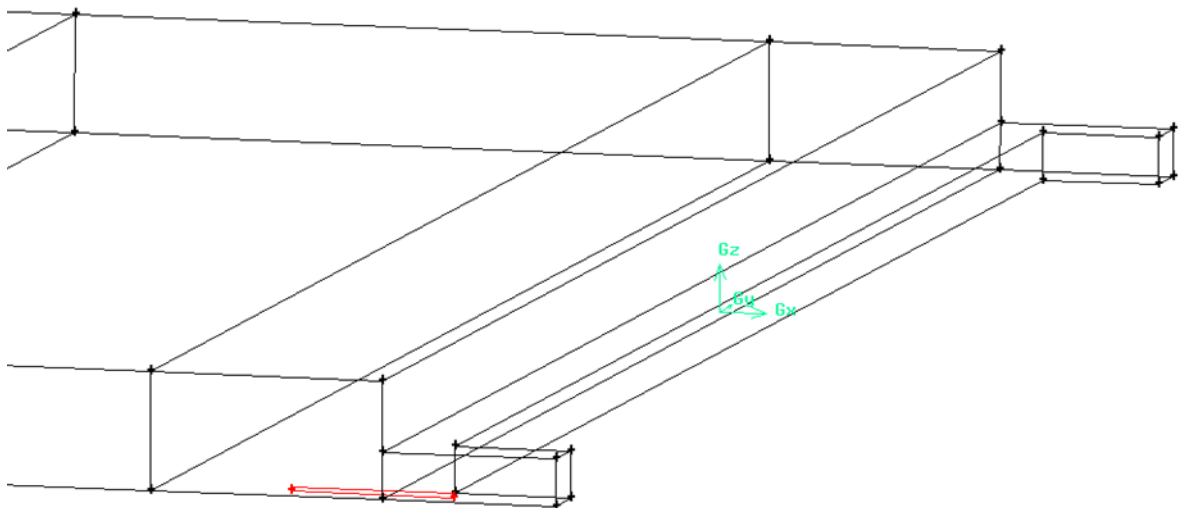


Figure 5.3 Pre-embedded pipe in the upper corner of goaf

The arrangement of pipe in the upper corner does not reflect the change of methane concentration associated with installation of pipe, but the main aim of this research paper does not focus on drainage effect from pipe installment, rather implementation of high-level drill holes in the fractures of overlying strata induced by longwall mining. Hence, under this configuration, the research aim is achieved.

---

## **5.7 Summary**

---

Having acquired results of the simulation from FLAC3D and FLUENT, the guideline of the methane drainage in the goaf area was proposed. The guidelines include arrangement of high-level and low-level boreholes in the overlying the goaf strata in fan-shaped configuration. The drilling parameters are as follow: set of 7 drilling sites, with 12 drill holes in each drilling site. The spacing between drilling fields was chosen to be 80 meters. With the aim of targeting overlapping zone of 20 meters, length of drill hole was chosen from 99 to 109 meters. Installation of pre-embedded pipe in the upper corner of goaf depth of embedment of 8 meters and diameter of pipe of 0.4 meters was suggested. All the suggested measures of methane drainage are in accordance with practice of methane drainage in Chinese coal mines.

---

## 6 Summary and conclusions

---

The understanding of development of cracks as well as movement of methane in goaf is of critical significance for effective design methane drainage and control to ensure safety in underground coal mine as well as drainage of gas as source of fuel.

To fully take advantage of depressurization of the overlying strata which induce the increase in permeability and imply the information for methane drainage, this study provided information on simulating the response of overlying strata to advance of working face by means of FLAC3D software. Analyzing evolution of stress, displacement and plasticity with advancing of working face, the fracture development zone was established according to its influence scope and trend.

The outcome of simulation presented the development of three zones in the funnel-shaped form in overlying the void strata: caving zone, fractured zone and bending subsidence zone. The results of the simulation presented the approximate zone where fractures are anticipated in the overlying strata with stress values in the zone ( $-5 \cdot 10^6$  MPa) and ( $1.0709 \cdot 10^6$  MPa), when 200 m of coal are excavated. What is more, the outcome of the simulation signified the increase of fractured zone with proceeding of excavation related to relief of pressure. Moreover, the results of simulation displayed formation of fractures mainly in the overlying strata above longwall panel in “O”-shaped form and approximate height of fractured zone was found out to be 40 meters.

It can be concluded that pressure relief after mining coal seam №7 changed the stress relief of overlying strata causing the increase in permeability of goaf in the form of fissure development. Consequently, the gas desorbed due to the impact of pressure relief will innately flow upwards to the newly formed fractures of overlying strata. Thus, the fissures of overlying strata will act as reservoir for accumulation of gas. The need for drainage of pressure-relief methane arises. Based on the notion that the height if the final hole should be adjusted in accordance with overburden strata structure, the drill holes were designed to be targeted within the boundary of caving and fractured zones. Based on the results of simulation by FLAC3D, the allocation of high-level and low-level drill-hole design was put forward so that boreholes would be set in “O”-shaped fracture zone in overlying strata. The drill-hole arrangement of 7 drill sites with 12 drill holes in each site and spacing of drilling fields 80 meters, length of drill hole ranging between 99 to 109 meters was established.

What is more, this study shed some light upon insight of methane movement inside the goaf. The flow of methane in the goaf area was examined through implementation of computational fluid dynamics FLUENT software. The results of simulation detected the region of low-velocity and high gas concentration in the upper corner of goaf area, thus, making the area prone to gas accidents. In order to reduce risk of gas accidents in the upper corner, buried pipe installation design was proposed with buried depth of 8 meters and diameter of 0.4 meters.

Further suggestions to improve the research outcomes are suggested such as: installation of buried pipe under varied pressure conditions and different embedded depths to monitor the change of methane concentration and through analyzing results establishment of best position in accordance with simulation results. Among limitations of the results are no precise location of high methane concentration in relation to working face. Further verification of the results of FLAC3D could be obtained through field test monitoring of the overlying strata as it is done in some research papers.

Nevertheless, the study exhibits generalization in insight of formation of three-zone of overlying strata, the development zone of cracks of overlying strata and identification of high-methane concentration zone in the upper corner of goaf area as well as theoretical guidance for methane drainage. The research outcomes can be regarded as preliminary basis for further work in the future. The results of the simulations can be regarded as site-specific and may be of use to study other problem-solving research in Kailuan group contribute to the knowledge of design of methane drainage under similar conditions.

---

## 7 Bibliography

---

1. Cai, Y., Liu, D., Mathews, J., Pan, Z., Elsworth, D., Yao, Y., Li, J. and Guo, X. (2014). Permeability evolution in fractured coal — Combining triaxial confinement with X-ray computed tomography, acoustic emission and ultrasonic techniques. *International Journal of Coal Geology*, [online] 122, pp.91-104. Available at: <https://www.sciencedirect.com/science/article/pii/S0166516213002796#bb0240> [Accessed 25 Apr. 2018].
2. Cempa-Balewicz, M., Jacek Łączny, M., Smoliński, A. and Iwaszenko, S. (2013). Equilibrium Model of Steam Gasification of Coal. *Journal of Sustainable Mining*, [online] 12(2), pp.21-28. Available at: <https://www.sciencedirect.com/science/article/pii/S2300396015300549> [Accessed 16 Mar. 2018].
3. Ding, H., Jiang, Z. and Zhu, Q. (2012). Optimized Parameters and Forecast Analysis of High-position Hole for Goaf Gas Drainage. *Procedia Engineering*, [online] 45, pp.305-310. Available at: <https://www.sciencedirect.com/science/article/pii/S1877705812031748> [Accessed 17 Apr. 2018].
4. Duan, S., Xu, X. (2012). Numerical analysis on ground displacement at mined-out area of Yuecheng reservoir project. *Advanced Materials Research*, [online] vols. 594-597 pp.194-197. Available at: <https://www.scientific.net/AMR.594-597.194> [Accessed 30 May 2018].
5. Esterhuizen, G.S., Karacan, C.O., (2005). Development of Numerical Models to Investigate Permeability Changes and Gas Emission around Longwall Mining Panel. In Proceedings of the 40th U.S. Symposium on Rock Mechanics. Anchorage, Alaska, June 25-29, 2005. American Rock Mechanics. 1-13.
6. Follington, I. and Isaac, A. (1990). Failure zone development above longwall panels. *Mining Science and Technology*, [online] 10(2), pp.103-116. Available at: <https://www.sciencedirect.com/science/article/pii/0167903190901229> [Accessed 10 Apr. 2018].
7. Fortin, J., Schubnel, A. and Guéguen, Y. (2005). Elastic wave velocities and permeability evolution during compaction of Bleurswiller sandstone. *International Journal of Rock Mechanics and Mining Sciences*, [online] 42(7-8), pp.873-889. Available at: <https://www.sciencedirect.com/science/article/pii/S1365160905000699> [Accessed 13 Apr. 2018].
8. Guo, H., Yuan, L., Shen, B., Qu, Q. and Xue, J. (2012). Mining-induced strata stress changes, fractures and gas flow dynamics in multi-seam longwall mining. *International Journal of Rock Mechanics and Mining Sciences*, [online] 54, pp.129-139. Available at: <https://www.sciencedirect.com/science/article/pii/S1365160912001037#s0085> [Accessed 20 Apr. 2018].
9. Guo, H., Todhunter, C., Qu, Q. and Qin, Z. (2015). Longwall horizontal gas drainage through goaf pressure control. *International Journal of Coal Geology*, [online] 150-151, pp.276-286. Available at: <https://www.sciencedirect.com/science/article/pii/S0166516215300495#s0015> [Accessed 20 Apr. 2018].
10. Guo, H. and Yuan, L. (2015). An integrated approach to study of strata behaviour and gas flow dynamics and its application. *International Journal of Coal Science & Technology*, [online] 2(1), pp.12-21. Available at: <https://link.springer.com/article/10.1007/s40789-015-0059-0#citeas> [Accessed 25 Feb. 2018].
11. Karacan, C., Ruiz, F., Cotè, M. and Phipps, S. (2011). Coal mine methane: A review of capture and utilization practices with benefits to mining safety and to greenhouse gas reduction. *International Journal of Coal Geology*, [online] 86(2-3), pp.121-156. Available at:



- <https://www.sciencedirect.com/science/article/pii/S0166516211000437> [Accessed 29 Apr. 2018].
12. Karmis, M., Triplett, T., Haycocks, C., Goodman, G., 1983. Mining subsidence and its prediction in an Appalachian coalfield. *Rock Mechanics: Theory, Experiment, Practice*. Proc. 24th US Symp. Rock Mechanics, 20–23 June 1983, Texas A&M University. Balkema, Rotterdam, pp. 665–675.
  13. Karacan, C., Esterhuizen, G., Schatzel, S. and Diamond, W. (2007). Reservoir simulation-based modeling for characterizing longwall methane emissions and gob gas venthole production. *International Journal of Coal Geology*, [online] 71(2-3), pp.225-245. Available at: <https://www.sciencedirect.com/science/article/pii/S0166516206001625#bib12> [Accessed 5 May 2018].
  14. Laubach, S., Marrett, R., Olson, J. and Scott, A. (1998). Characteristics and origins of coal cleat: A review. *International Journal of Coal Geology*, [online] 35(1-4), pp.175-207. Available at: <https://www.sciencedirect.com/science/article/pii/S0166516297000128#BIB50> [Accessed 25 Apr. 2018].
  15. Li, L. (2013). Technology of gas drainage with high drilling boreholes. *China Science and Technology*, 41 (S1): pp, 92-94 (in Chinese).
  16. Li, Y. (2018). Upper corner gas control based on high level directional long borehole. *Coal science and technology*, 46(01), pp. 215-218 (in Chinese).
  17. Meng, Z., Shi, X. and Li, G. (2016). Deformation, failure and permeability of coal-bearing strata during longwall mining. *Engineering Geology*, [online] 208, pp.69-80. Available at: <https://www.sciencedirect.com/science/article/pii/S0013795216301223> [Accessed 25 Mar. 2018].
  18. Moll, A.T.J. 1993, “A study of optimization methods applied to methane recovery and mine ventilation systems”, PhD thesis, University of Nottingham, Nottingham, United Kingdom.
  19. Nie, M. (2008). Application of gas drainage technology with high level boreholes in Zhuzhuang Mine. *Coal science and technology*, (08) pp.55-57 (in Chinese).
  20. Palchik, V. (2003). Formation of fractured zones in overburden due to longwall mining. *Journal of Environmental Geology*, [online] 44(1), 28-38. Available at: <https://link.springer.com/article/10.1007/s00254-002-0732-7> [Accessed 7 Mar. 2018].
  21. Palchik, V. (2002). Influence of physical characteristics of weak rock mass on height of caved zone over abandoned subsurface coal seam. *Journal of Environmental Geology* 42 (1), pp. 92-101.
  22. Qin, Z., Yuan, L., Guo, H. and Qu, Q. (2015). Investigation of longwall goaf gas flows and borehole drainage performance by CFD simulation. *International Journal of Coal and Geology*, [online] 150-151, pp. 51-63. Available at: <https://www.sciencedirect.com/science/article/pii/S0166516215300409#bb0080>
  23. Qu, Q., Xu J., Wu, R. and Hu G. (2015). Three-zone characterization of coupled strata and gas behaviour in multi-seam mining. *International Journal of Rock Mechanics and Mining Sciences*, [online] 78, pp. 91-98. Available at: <https://www.sciencedirect.com/science/article/pii/S1365160915001252> [Accessed 5 Mar. 2018].
  24. Rowland, J., Manga T., and Rose, T. (2008). The influence of poorly interconnected fault zone flow paths on spring geochemistry. *Geofluids*, 8, pp. 93-101.
  25. Shi, B. and Liu, Z. (2008). Numerical Simulation of Deformation Characteristics of Overburden Coal Seam Excavated by Protective Layer. *Journal of China Coal Society*, (01), pp. 17-22. (in Chinese).

26. Sui, W., Zhang, D., Cui, Z., Wu, Z. and Zhao, Q. (2014). Environmental implications of mitigating overburden failure and subsidences using paste-like backfill mining: a case study. *International Journal of Mining, Reclamation and Environment*, [online] 29(6), pp.521-543. Available at: <https://www.tandfonline.com/doi/full/10.1080/17480930.2014.969049> [Accessed 4 May 2018].
27. Tian-xuan, H., Zhi-chao, J. and Feng, L. (2012). Optimization of Goaf Gas Drainage Parameters Based on Numerical Simulation Studying Fracture in Overlying Strata. *Procedia Engineering*, [online] 43, pp.269-275. Available at: <https://www.sciencedirect.com/science/article/pii/S1877705812030573> [Accessed 29 Apr. 2018].
28. Turchainov, I., Iofis M., Kasparyan E. (1977). Principles of rock mechanics. Nedra, Leningrad (in Russian)
29. Wang, S., Elsworth, D. and Liu, J. (2013). Permeability evolution during progressive deformation of intact coal and implications for instability in underground coal seams. *International Journal of Rock Mechanics and Mining Sciences*, [online] 58, pp.34-45. Available at: <https://www.sciencedirect.com/science/article/pii/S1365160912002018> [Accessed 7 Apr. 2018].
30. Wang, L., Cheng, Y. and Liu, H. (2014). An analysis of fatal gas accidents in Chinese coal mines. *Safety Science*, [online] 62, pp.107-113. Available at: <https://www.sciencedirect.com/science/article/pii/S092575351300194X> [Accessed 4 Mar. 2018].
31. Wang, G., Wu, M., Wang, R., Xu, H. and Song, X. (2017). Height of the mining-induced fractured zone above a coal face. *Engineering Geology*, 216, pp.140-152.
32. Whittles, D., Lowndes, I., Kingman, S., Yates, C. and Jobling, S. (2006). Influence of geotechnical factors on gas flow experienced in a UK longwall coal mine panel. *International Journal of Rock Mechanics and Mining Sciences*, [online] 43(3), pp.369-387. Available at: <https://www.sciencedirect.com/science/article/pii/S1365160905001139?via%3Dihub> [Accessed 5 Mar. 2018].
33. Xu, X., Zhang, N. and Tian, S. (2012). Mining-induced movement properties and fissure time-space evolution law in overlying strata. *International Journal of Mining Science and Technology*, [online] 22(6), pp.817-820. Available at: <https://www.sciencedirect.com/science/article/pii/S2095268612002017> [Accessed 20 Apr. 2018].
34. Xu, Z., Sun, Y., Dong, Q., Zhang, G. and Li, S. (2010). Predicting the height of water-flow fractured zone during coal mining under the Xiaolangdi Reservoir. *Mining Science and Technology (China)*, [online] 20(3), pp.434-438. Available at: <https://www.sciencedirect.com/science/article/pii/S1674526409602222> [Accessed 28 Mar. 2018].
35. Zhang, J., Cliff, D., Xu, K. and You, G. (2018) (a). Focusing on the patterns and characteristics of extraordinarily severe gas explosion accidents in Chinese coal mines. *Process Safety and Environmental Protection*, [online] 117, pp.390-398. Available at: <https://www.sciencedirect.com/science/article/pii/S0957582018301496> [Accessed 7 May 2018].
36. Zhang, Y., Zhang, X., Li, C., Liu, C. and Wang, Z. (2011). Methane moving law with long gas extraction holes in goaf. *Procedia Engineering*, [online] 26, pp.357-365. Available at: <https://www.sciencedirect.com/science/article/pii/S1877705811050223> [Accessed 19 Mar. 2018].
37. Zhang, R., Cheng, Y., Zhou, H., Yuan, L., Li, W., Liu, Q., Jin, K. and Tu, Q. (2018). (b). New insights into the permeability-increasing area of overlying coal seams disturbed by the mining of coal. *Journal of Natural Gas Science and Engineering*, [online] 49, pp.352-364. Available at:

[https://www.researchgate.net/publication/321384331\\_New\\_insights\\_into\\_the\\_permeability-increasing\\_area\\_of\\_overlying\\_coal\\_seams\\_disturbed\\_by\\_the\\_mining\\_of\\_coal](https://www.researchgate.net/publication/321384331_New_insights_into_the_permeability-increasing_area_of_overlying_coal_seams_disturbed_by_the_mining_of_coal) [Accessed 20 Apr. 2018].

38. Zhang, P. (2012). Numerical simulation of methane delivery law in U type ventilation work face gob. *Energy Procedia*, [online] 14, pp.632-636. Available at: <https://www.sciencedirect.com/science/article/pii/S1876610211044079?via%3Dihub> [Accessed 15 Apr. 2018].
39. Zhang, M., Wu, S. and Wang, Y. (2012). Research and application of drainage parameters for gas accumulation zone in overlying strata of goaf area. *Safety Science*, [online] 50(4), pp.778-782. Available at: <https://www.sciencedirect.com/science/article/pii/S0925753511002062> [Accessed 14 Apr. 2018].

---

## 8 List of Figures

---

Figure 2.1 The location of Qianjiaying Coal Mine.....	5
Figure 2.2. The ventilation layout of the 2874 W working face.....	6
Figure 3.1. Division of three zones adopted from (Zhang et al., 2012).....	8
Figure 3.2. The failure and deformation experienced in overlying strata during longwall mining adopted from (Meng et al., 2016).....	11
Figure 3.3. Numerical simulation model.....	14
Figure 3.4. Initial vertical stress distribution.....	14
Figure 3.5. Initial distribution of horizontal stresses.....	15
Figure 3.6. The vertical stress profile of the model along direction of strike after mining out 20m.....	17
Figure 3.7. The vertical stress profile of the model along direction of the dip after mining out 20m.....	17
Figure 3.8. The vertical stress profile of the model along strike direction after mining out 100 m.....	18
Figure 3.9. The vertical stress profile of the model along the dip direction after mining out 100 m.....	18
Figure 3.10. The vertical stress profile of the model along direction of strike after mining out 200m.....	19
Figure 3.11. The vertical stress profile of the model along the dip direction after mining out 200m.....	19
Figure 3.12. Vertical displacement of the model along strike direction after mining out 20m.....	21
Figure 3.13. Vertical displacement profile of the model along strike direction after extracting 100 m.....	22
Figure 3.14. Profile of vertical displacement the model along strike direction after mining out 200m.....	22
Figure 3.15. Profile of vertical displacement along dip direction after mining out 20 m.....	23
Figure 3.16. Profile of vertical displacement of model along dip direction after mining out 100 m.....	23
Figure 3.17. Profile of vertical displacement of model along dip direction after mining out 200 m.....	24
Figure 3.18. The model of damage state of the surrounding strata after mining out 20 m.....	25
Figure 3.19. The model of damage state of the surrounding strata after mining out 100 m.....	26
Figure 3.20. The damage state of the surrounding strata along dip direction after mining out 200 m.....	26

Figure 3.21. The damage state of the surrounding strata along strike direction after mining out 20m.....	27
Figure 3.22. The damage state of the surrounding strata along strike direction after mining out 100m.....	27
Figure 3.23. The damage state of the surrounding strata along strike direction after mining out 200 m.....	28
Figure 4.1 Geometric model of goaf.....	31
Figure 4.2. Distribution of velocity.....	36
Figure 4.3. The distribution of velocity presented in vectors in the inlet.....	36
Figure 4.4 The distribution of velocity presented in vectors in the upper corner of goaf.....	37
Figure 4.5 The distribution of mass fraction of methane.....	38
Figure 4.6. Distribution of pressure.....	39
Figure 5.1 The relationship between the parameters of the drill hole.....	44
Figure 5.2 The design of high-level and low-level drill holes in the overlying strata of goaf.....	53
Figure 5.3 Pre-embedded pipe in the upper corner of goaf.....	55

---

## 9 List of Tables

---

Table 3.1. Empirical expressions between height of the overlying fractured zone (H <sub>d</sub> ) and the mining thickness (M) used in China.....	9
Table 3.2. Input data for simulation.....	13
Table 3.3. Mechanical and physical properties of the model.....	16
Table 5.1. Designed drilling parameters.....	53



中国矿业大学 (北京)

China University of Mining & Technology-Beijing

### Thesis Grade

Thesis topic: The Development of Fractures in Overlying Strata and Design of Methane Drainage on 2874W working face in Qianjiaying Coal Mine

Author: Gulzhan Yedigeyeva

Supervisor

Zhu Hongqing

Grade 91

signature

Co-supervisor

Carsten Drebenstedt

Grade

signature



中国矿业大学 (北京)

China University of Mining & Technology-Beijing

**Thesis Grade**

**Thesis topic: The Development of Fractures in Overlying Strata and Design of Methane Drainage on 2874W working face in Qianjiaying Coal Mine**

Author: Gulzhan Yedigeyeva

Review expert Li Feng

Grade 90

signature

A handwritten signature in black ink, appearing to be 'Li Feng'.